UNIVERSITY OF CALIFORNIA, SAN DIEGO

Hail Ice Impact of Lightweight Composite Sandwich Panels

A Thesis submitted in partial satisfaction of the
requirements for the degree of Master of Science

in

Structural Engineering

by

Sean Dustin Luong

Committee in charge:

Professor Hyonny Kim, Chair
Professor Chiara Bisagni
Professor Yael Dahlia Van Den Einde

2014

The Thesis of Sean Dustin Luong is approved, and it is acceptable in quality and form for publication on microfilm and electronically:

_____

_____

_____
Chair

University of California, San Diego

2014

TABLE OF CONTENTS

LIST OF ABBREVIATIONS

BVID – Barely visible impact damage

CAI – Compression after impact

CFRP – Carbon fiber reinforced polymer

PCF – Pounds per cubic foot

SHI – Simulated hail ice

LIST OF FIGURES

LIST OF TABLES

ACKNOWLEDGEMENTS

I would like to thank Professor Hyonny Kim for all the opportunities he has provided me. He has provided me an environment in which I have been able to thrive academically and professionally. I will be eternally grateful for everything he has taught me and helped me to achieve.

I would also like to thank Professor Lelli Van Den Einde for her guidance throughout my undergraduate career at UC San Diego. Without her help, I would not be where I am today.

I would like to thank all the professors that I have worked with or studied with through these years, because they have all contributed to my education as a person and as an engineer and driven me to succeed.

Lastly, I would like to thank the other students in Professor Kim's lab for all the help they have given me in accomplishing my research as well as the support they have provided to me in life in general.

ABSTRACT OF THE THESIS

Hail Ice Impact of Lightweight Composite Sandwich Panels

by

Sean Dustin Luong

Master of Science in Structural Engineering

University of California, San Diego, 2014

Professor Hyonny Kim, Chair

There is a growing demand for the usage of composite sandwich structures in the aircraft industry. Aircraft may suffer damage from a variety of impact sources such as ground service equipment, runway debris, bird strike, or hail ice. The damage response of hail ice impacts on composite sandwich structures is not well understood and they can

often result in core damage without visually detectable surface damage. This seed damage may grow and lead to large-scale failure of the structure through repetitive operational loading, such as ground-air-ground cycles of aircraft (causes core internal pressurization). Therefore, it is necessary to understand the types of damage that can occur as a result of impacts.

This study explores the effect of high velocity hail ice impact on damage formation in lightweight composite sandwich panels, particularly at a level that produces barely visible external damage. Panels consisting of two different facesheet thicknesses (1.19 and 1.87 mm) were impacted at angles of 25, 40, and 90 degrees at speeds of 25 and 50 m/s. The tests revealed three different core damage modes. Any level of measurable surface damage was an indicator of the presence of internal core damage, but internal damage could also be present without measurable surface damage. Thus, visual inspection alone was not a reliable method of damage detection. No clear relationship was found between impact energy levels and internal damage state since, for example, both 83 and 20.5 J tests produced core fracture, while a 16 J test did not produce any core damage. All core damage occurred at a depth of 3-5 mm from the impact-side facesheet.

.

1 INTRODUCTION

1.1 MOTIVATION

Today, composite materials are being utilized much more widely than in the past. Of the total weight in the Boeing 747, only 1% came from composite materials, while for the Boeing 757/767 and 777, the total weight came from 3% and 11%, respectively. The latest 787 Dreamliner consists of 50% composite materials [1, 2]. More specifically, composite sandwich panels are of interest for their high bending rigidity (more stable structure) and high strength-to-weight ratio [3]. Composite sandwich panels are structures that utilize composite laminates as facesheets separated by a lightweight core (usually a foam or honeycomb material) which increases the bending rigidity without too much increase in weight. They are analogous to I-beams where the facesheets carry axial and bending loads (like the flanges) and the core carries the shear loads (like the web) [4]. However, several potential disadvantages arise when using composites over traditional metals. This is because their impact characteristics are not well understood, particularly when impacted by blunt sources creating internal damage with little or no exterior visibility; such impact events would leave a telling dent or crack on a metal surface.

An in-service aircraft may encounter impacts from a variety of projectiles such as blunt sources from ground service vehicles and runway debris, hail impact, or bird strike prior to take off, while the plane is in flight, and during landing. Aircraft components that are particularly vulnerable to bird or hail impact include the fuselage, wing or tail leading

edges, stabilizers, radomes, nacelles, and turbine blades. Furthermore, the worldwide cost of such bird and hail impact damage exceeds 3 billion USD per year [2, 5]. The varying types of projectiles and range in speeds at which impacts may occur can result in different damage modes that significantly reduce the residual strength such as fiber failure, matrix cracking, delamination, facesheet disbonding, core crushing, and the interaction between any of these damage modes [6]. Such damage may grow and eventually lead to sudden large-scale failure due to repeated loading cycles. For example, the pressure loading/unloading process during the repetitive ground-air-ground cycle of aircraft can induce disbonding of the sandwich facesheet. Often, such damage may initiate at a very small scale (mm) or below the facesheet surface and cannot be visually detected from the exterior [7]. Another dangerous possibility is if the initial damage was due to human error (such as a tool drop or vehicle collision), it could go unnoticed or unreported, potentially leading to significant failure in the future.

This work focuses on the threat of hail ice impact. In places where severe storms are common, it is not unusual for hail storms to produce tennis ball-sized and larger projectiles. Figure 1.1.1 shows examples of such projectiles from a recent hail storm in Nebraska, USA [8].

Figure 1.1.1. Hailstones from 06/04/2014 Nebraska storm [8]**.**

Hail ice poses a dangerous threat to aircraft as they can vary in size and speed of impact. At a minimum, they may impact aircraft on the ground at falling terminal velocities of 30-50 m/s, but at the other end of the spectrum they may impact aircraft at in-flight speeds of 200 m/s or greater. The United States Air Force reported 272 hail impact events from 1951 to 1959, with 46% taking place at in-flight speeds [9]. Figure 1.1.2 summarizes this data and shows that most cases consisted of hail that were less than 26 mm in diameter [9]. Though these data were collected many years ago, it provides insight on the possible distribution of hail threats today.

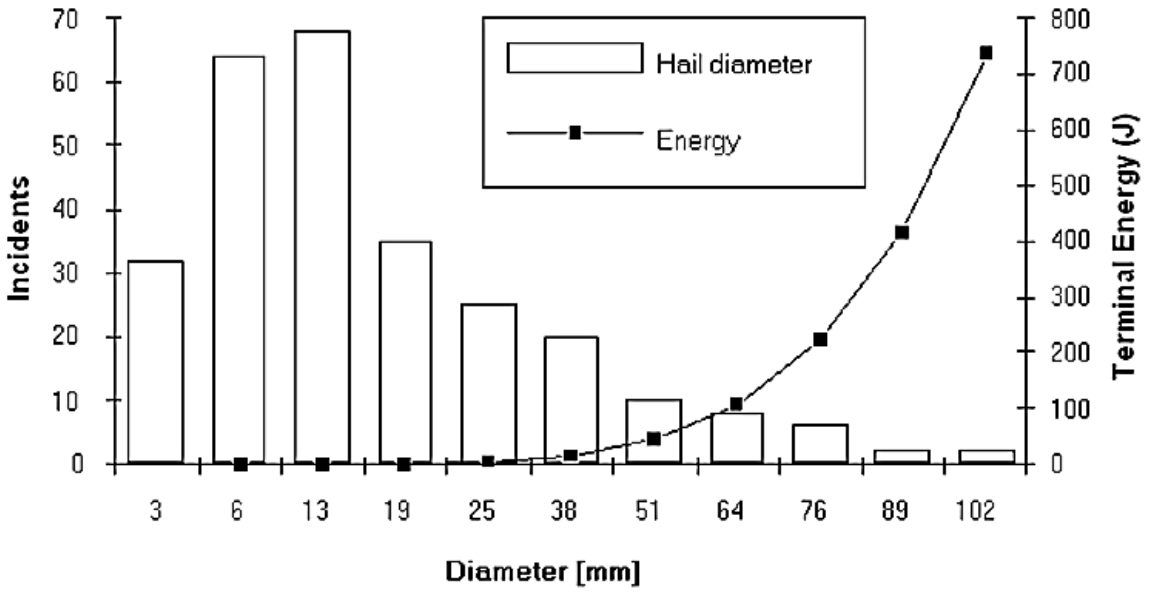

Figure 1.1.2. Distribution of 272 damaging hail impact events

Despite the increasing usage of composite honeycomb sandwich structures and prevalence of hail impact threats, there is little to no research investigating the effects of hail impact damage on composite sandwich structures. Therefore, it is imperative to understand what type of damage to expect after an ice impact event in order to determine the realistic levels of damage which may exist, with little or no visual detectability, as well as provide guidance on subsequent inspection and repair practices that must be considered following a hail ice impact event.

1.2 Previous Work

Most work in the past involving composite sandwich panels focused on low-velocity normal impacts, usually achieved through various drop weight mechanisms.

Amir et al. [4] conducted low velocity drop weight impact testing on glass fiber/epoxy polypropylene honeycomb sandwich panels with varying core thicknesses and found that major failures tended to take place in the upper region (towards the impact side) of the sandwich structures, and thicker core structures exhibited higher resistance to out-of-plane deformation for low velocity impact. On the other hand, Othman and Barton [10] conducted quasi-static and low-velocity drop weight impact tests on carbon/epoxy Nomex honeycomb sandwich panels of different thicknesses and found that the impact tests produced highly localized damage, and thus the varying thicknesses were found to contribute very little to the overall energy absorbing capabilities of the sandwich structure. The difference in conclusions is likely due to the fact that Othman and Barton's impact tests involved impact energies of 1800 J while the tests conducted by Amir et al. involved impact energies two orders of magnitude smaller, ranging from 15-45 J.

Anderson and Madenci [11] also utilized drop weight low velocity impact tests on a variety of different composite sandwich panels. Their impact tests had energy levels ranging from 8 to 26 J and resulted in specimens that did not visually exhibit much surface damage but after sectioning, revealed significant core damage such as cell wall buckling and core crushing adjacent to the impact site. This suggests that visual inspections can be misleading since significant internal damage may be hidden. They also investigated a number of panel configurations: 3-ply and 6-ply facesheets, foam and honeycomb cores, as well as high density and low density versions of each of the core types, and found that despite thicker and denser specimens requiring higher energy levels to produce damage, similar types of damage modes were present in all configurations.

Due to the small size of their specimens (76.2 mm x 76.2 mm), an additional type of damage occurred where the core specimens exhibited cracking or tearing from the center of the laminate to the edges. Therefore, it is important to investigate the effects of impact on larger specimens in order to observe local effects that are not obscured by other undesirable defects.

McQuigg et al. [6] conducted drop weight low velocity impact tests on carbon/epoxy Nomex honeycomb sandwich panels with increasing levels of energy and two different core densities of 3 pounds per cubic foot (pcf) and 6 pcf. These tests resulted in standard damage modes of skin penetration and core crushing, but interestingly the depth of core crushing was approximately the same level at all the different impact energies. As expected, the higher density core resulted in a higher impact resistance. They also ran compression after impact (CAI) tests to determine residual strength and found that compared with the compressive strength of undamaged specimens, even small amounts of damage resulted in a noticeable decrease in panel strength. However, increasing levels of damage resulted in smaller decreases in residual strength.

Raju et al. [12] similarly utilized drop weight tests and CAI testing to study carbon/epoxy Nomex honeycomb core sandwich panels at escalating levels of impact energy. Through non-destructive C-scans and destructive sectioning, they found the size of the residual dent region on the surface was always less than or equal to the damage region revealed through C-scans, and this damage region was always smaller than the core damage region except when facesheet fracture occurred. Five damage states were

identified from escalating levels of impact energy: initiation of damage (delamination) in facesheet and initiation of core crushing, damage progression through the facesheet and actual core crushing, facesheet fracture, penetration of facesheet and core crushing/consolidation, and finally damage initiation in the bottom facesheet. However, the facesheet to core bond remained intact in all of these cases.

Presently there is virtually no work done examining the effects of hail impact on composite sandwich structures though there has been significant work in studying hail impact on carbon/epoxy panels. Kim et al. [13] conducted high velocity hail impact tests (from 30-200 m/s) on carbon/epoxy panels and found that the failure threshold energy of the panels scaled linearly with panel thickness, the failure threshold energy of glancing impacts were scalable from normal impacts with a trigonometric relationship, and the boundary conditions of the panel do not have a large influence on the experimental results due to the localized effect of the dynamic impact. Rhymer et al. [14] also conducted high velocity hail ice impact tests on carbon/epoxy panels of different thicknesses and material architecture using projectiles with different diameters. There were cases in which similar impact energy levels produced results with damage and results without damage, and this was likely due to variations in the panels and ice projectiles. The failure threshold energy was directly related to the projectile diameter and the panel thickness, and formation of delamination is mostly governed by matrix material properties rather than the fiber architecture/properties. While these studies are more aligned with the experimental research conducted in the present study, they focused on the energy levels required for initiation of delamination damage, which provide a good

starting point for the research described herein focused on characterizing the damage formation in composite sandwich structures due to hail ice impact.

1.3 OBJECTIVES

The present study seeks to identify the possible damage states that may result from hail impact tests at different angles and speeds on lightweight composite sandwich panels with varying facesheet thicknesses. Of particular interest is the damage level in which either barely visible impact damage (BVID) or no visible damage exists together with significant internal core damage. The damage states will be characterized and quantified as much as possible in order to determine the correlation between various damage metrics and presence of internal core damage.

2 EXPERIMENTAL SETUP

2.1 FABRICATION OF HAIL ICE PROJECTILES

The projectiles used to conduct the experiments are simulated hail ice (SHI): from here on, the term “hail ice projectile” or “ice” refers to the SHI produced in the lab. These projectiles differ from natural hailstones as they are nearly spherical and ideally uniform. Natural hailstones can come in various shapes and sizes (see Figure 1.1.1), and larger ones usually contain multiple layers due to the way they form through a cyclic process of rising [9] and falling while accumulating water in the atmosphere. Natural hail may also vary in density, but the SHI produced in this study are close to 0.9 g/cm^3. There are two common approaches to approximating natural hail ice, one is producing clear SHI that is similar to solid ice, while the other is producing cotton-filled SHI that is less dense and more tough; since the mechanical properties of natural hail ice has not been thoroughly studied, neither approach is considered to be more accurate [15]. The ASTM F320-10 [16] outlines a method in producing the cotton-filled SHI variety that utilizes 12% cotton by weight. These experiments used the solid ice approach rather than the ASTM approach because the cotton-filled SHI were too tough for the lightweight test specimens and would consistently penetrate the facesheets. The hail ice projectiles were prepared using an aluminum split mold with 2 inch diameter hemispherical cavities and vent holes that allowed the molds to be filled with water and provided space for water expansion during the freezing process. After the mold halves were clamped together with c-clamps,

a syringe was used to fill the cavities with boiling hot de-ionized water. This would reduce the gas content of the water (which otherwise leads to the formation of voids) and caused the water to freeze faster due to the Mpemba Effect [17]. The mold was then placed in a freezer (lower than 5° F) for a period of at least 6 hours. Afterwards, the mold was opened and the hail ice projectiles were removed and acceptable ones were sealed in polyethylene bags and then placed back in the freezer. Any ice balls with noticeable cracks or uneven shape were disposed of and were not used for tests on panels. Figure 2.1.1 shows both halves of a mold prior to being filled with water.

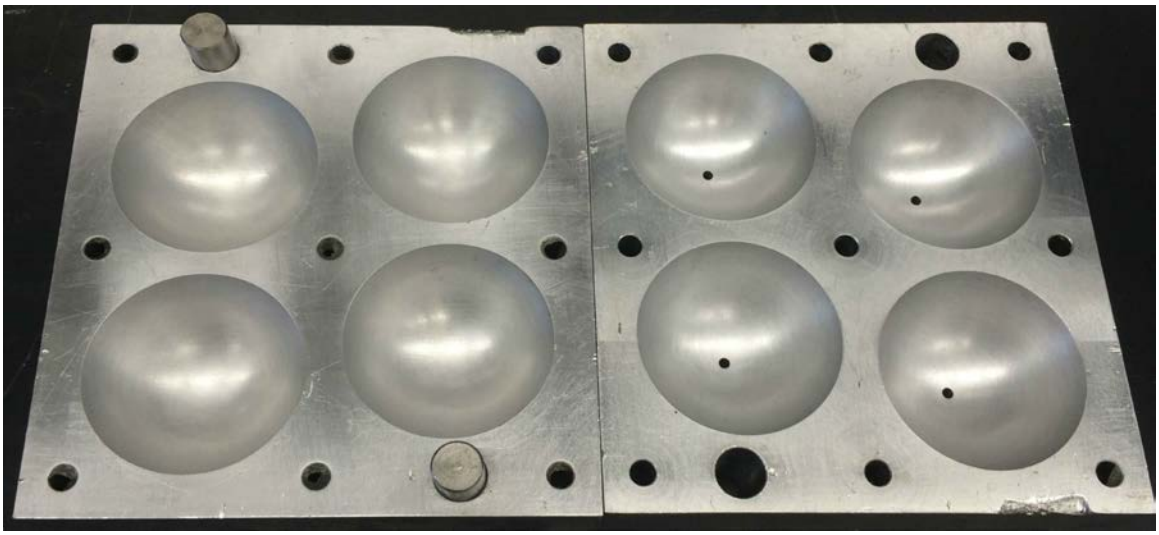

Figure 2.1.1. Split mold for 50.8 mm diameter hail ice projectile.

It is important for consistency to utilize uniform SHI, because the presence of any voids, such as air bubbles, could result in stress concentrations that eventually lead to fracturing or failure of the SHI before reaching the target. Learning to produce consistent hail ice projectiles was a process of trial and error because of the lack of documentation or a standard process. During early iterations, the ice would often fracture immediately

upon separation of the mold halves. This was hypothesized to be caused by overfilling the molds. As the water expands during freezing process, the mold exerts pressure on the projectile and the ice will be in a state of internal hydrostatic compression. Once the mold is separated, the confining pressure at the mold-sphere interface would be removed and the internal stresses of the ice would cause it to split. This was remedied by calculating exactly how much water needed to be removed in order to have a final target mass of 61g for 2.0 in. diameter. Although the mold would essentially be underfilled (in liquid phase), there would be no internal pressures upon removal. It was also easier and more consistent to fill the mold cavities to the brim of the fill hole and then remove a specific amount of water rather than trying to precisely inject a certain amount of water every time.

Another factor that would often cause failure of the ice during the removal process was temperature. It would be difficult to unscrew the C-clamps and separate the mold halves upon initial removal from the freezer due to the metal C-clamps shrinking. Therefore, the C-clamps would be warmed up with running water for approximately 15-30 seconds and they could be removed with relative ease. However, once the mold halves were separated, the ice would often firmly stick to the mold cavities making removal of the ice from the mold challenging. This was solved by running water on the bottom of the mold half that contained the ice to warm it up. It was important not to do this for too long because the rapid change in temperature could cause the ice to fracture, melt, or lose too much mass.

Finally, it was hypothesized that uniformness of cooling rate would have an impact on the formation of voids. Thus, holes were drilled around the circumference of

the mold cavities as seen in Figure 2.1.1 in order to allow for uniform cooling of the water in each cavity. Additionally, a layer of insulating cloth was placed on top of the molds in order to prevent the fill holes from freezing first and stopping the ice from being able to expand into the holes (which would lead to the aforementioned internal pressures). Despite all these precautions and measures taken to produce uniform SHI, a small percentage of the projectiles still fractured when they were launched through the gas gun, particularly at higher velocity.

SHI of 50.8 mm diameter were used for the scope of this study because 61.0 mm diameter ice consistently penetrated the front facesheet, which is well beyond the level of damage in which this investigation was focused on.

The importance of the SHI integrity cannot be understated; in the second image of Figure 2.1.2, it can be seen in the reflection highlighted by the yellow box that the SHI broke in half prior to impact. This led to a higher than usual level of crushing during impact which dissipated a lot of the energy. Although this test was a high velocity/energy test at 49.38 m/s and 75.24 J, it produced a dent of only 0.02 mm, whereas a test with similar conditions at 48.26 m/s produced a significantly noticeable dent because the SHI did not lose energy from breaking apart.

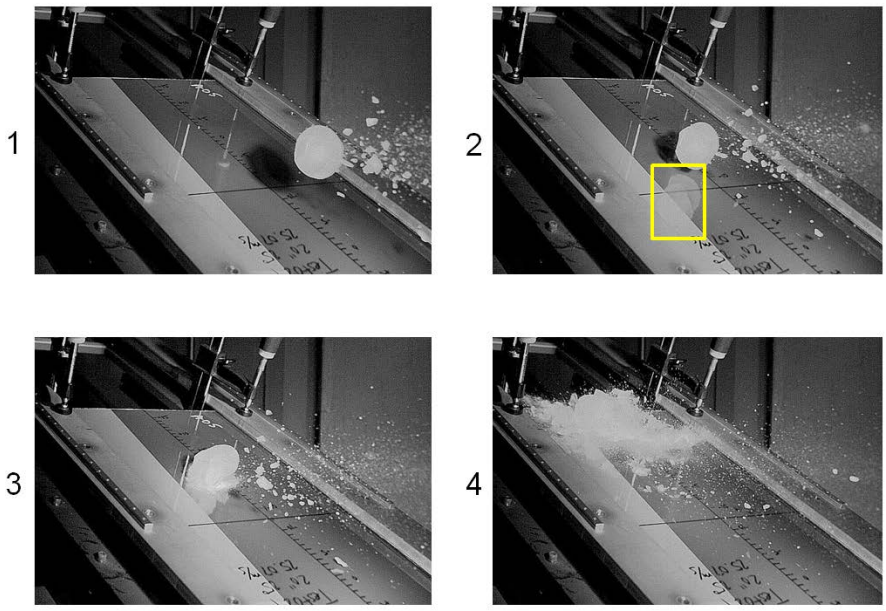

Figure 2.1.2. SHI cracked prior to impact, resulting in significantly reduced damage.

Though the SHI in Figure 2.1.3 broke upon impact, it did not completely crush like the one in Figure 2.1.2, and it resulted in a higher level of internal damage even though the test was a lower velocity/energy test at 25.46 m/s and 20.45 J. However, it should be noted that this specimen was impacted at a steeper angle of 40 degrees.

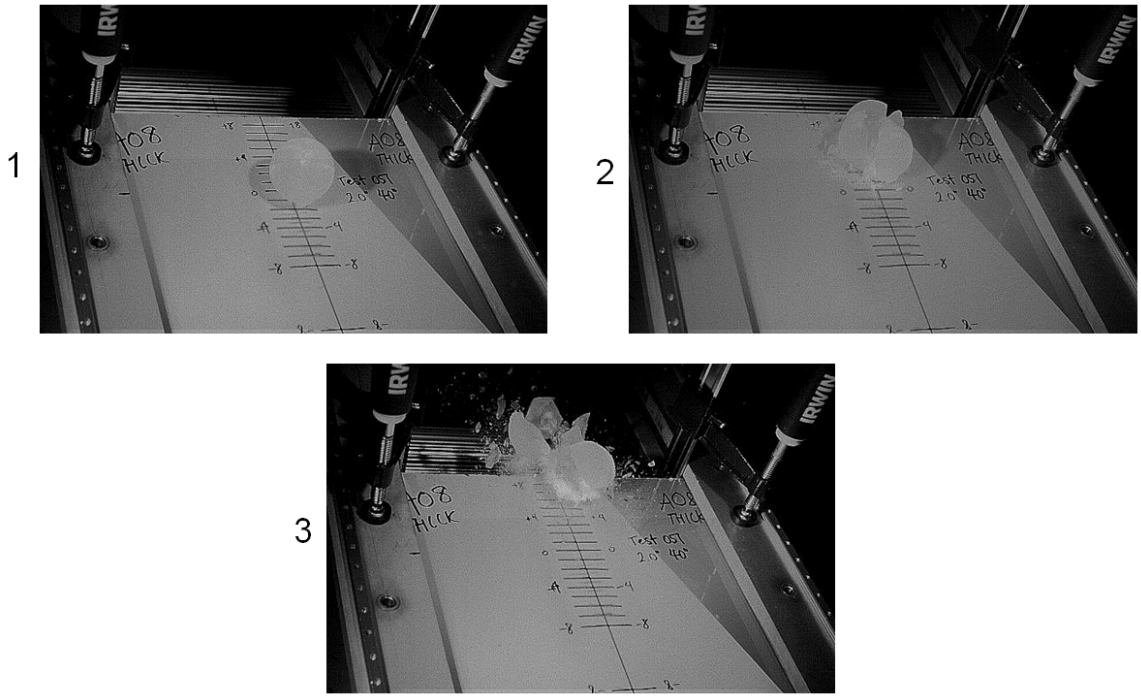

Figure 2.1.3. SHI intact prior to impact, but broke on impact, resulting in core damage without dent.

Finally, Figure 2.1.4 shows the case where the projectile stayed intact during the impact. Since the SHI did not break, no energy was lost and more of it was transferred into the target, which resulted in facesheet penetration.

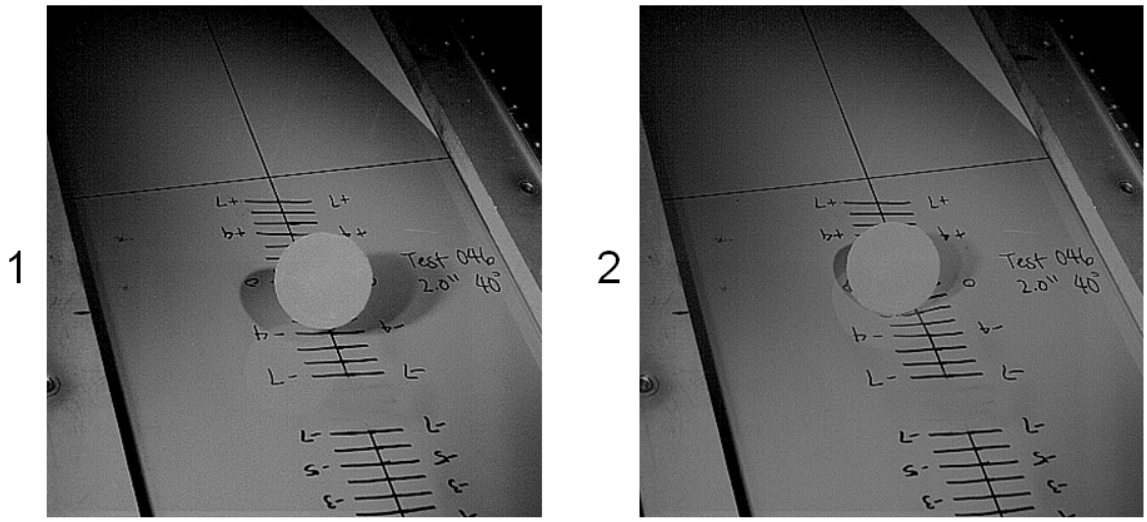

Figure 2.1.4. SHI did not break during impact, resulting in facesheet penetration.

Overall, SHI status was organized into two categories: intact during flight and fractured during flight. When the SHI fractured during flight, it tended to crush or break into smaller pieces upon impact, dissipating more energy than normal and reducing the amount of visible damage. However, a significant amount of internal core damage was still observed from an SHI impact that already fractured during flight. SHI that are intact during flight either fractured upon impact or stayed intact. The SHI that stay intact during flight and impact imparted the most damage upon the target, usually leaving a visible dent, if not penetrating the facesheet. The SHI that fractured upon impact only sometimes caused visible dents and internal core damage. A number of factors such as SHI quality (amount of voids/presence of cracks), stiffness of impacted facesheet, and higher incidence angles, that led to the probability of SHI fracture upon impact.

2.2 Fabrication of Sabots

Split foam sabots were utilized to maintain the straight trajectory of the projectiles through the barrel and to keep the SHI from melting by preventing contact with the barrel's metal surface. Upon exit, the two sabot halves would separate and were stopped by a steel plate with a 70.0 mm diameter hole, allowing only the projectile to pass through to the velocity measurement system and on to the target. Figure 2.2.1 shows this mechanism. Two rubber pads were placed on the sabot stop plate, which would extend the lifespan (allowing re-use) of the sabots for lower speed tests.

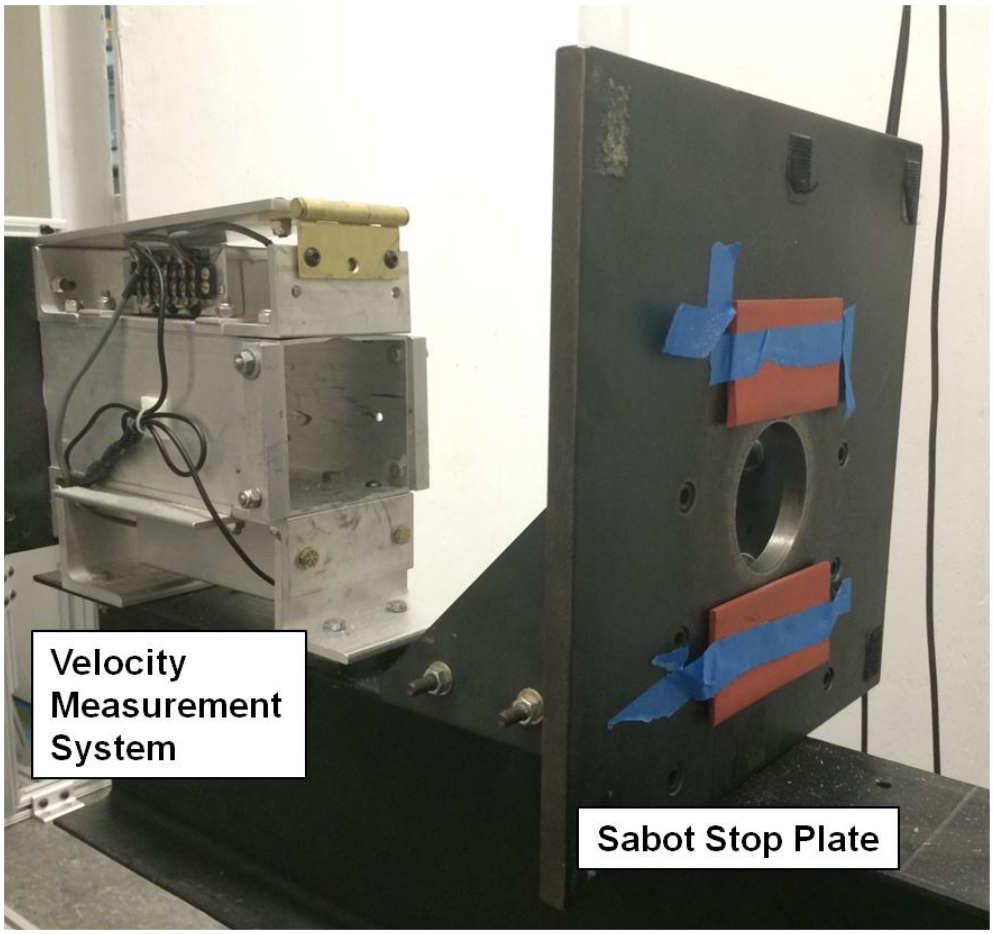

Figure 2.2.1. Sabot stop system as viewed from facing the direction of the target.

These sabots were made by filling the molds with Foam-It 5, a rigid polyurethane foam of 5 pcf density. The foam was left in the mold for a period of at least one hour for it to fully expand into the mold and to solidify. Afterwards, the mold was taken apart, and the sabot was cut down the center from top to bottom to form the two halves. These halves were held together with a rubber "v-seal" ring that secured the bottom of the sabot but still allowed the top to open up and release the projectile. Figure 2.2.2 shows a sabot more clearly.

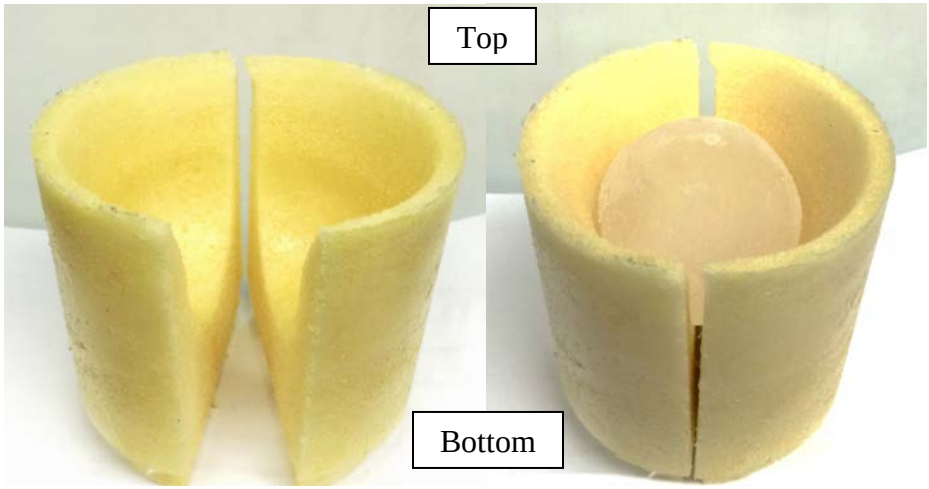

Figure 2.2.2. Polyurethane foam split sabot and 50.8 mm diameter SHI without v-seal ring.

2.3 Test Specimens

The panels used for the hail ice impact tests were obtained from an Airbus A320 rudder seen in Figure 2.3.1 that was removed from service.

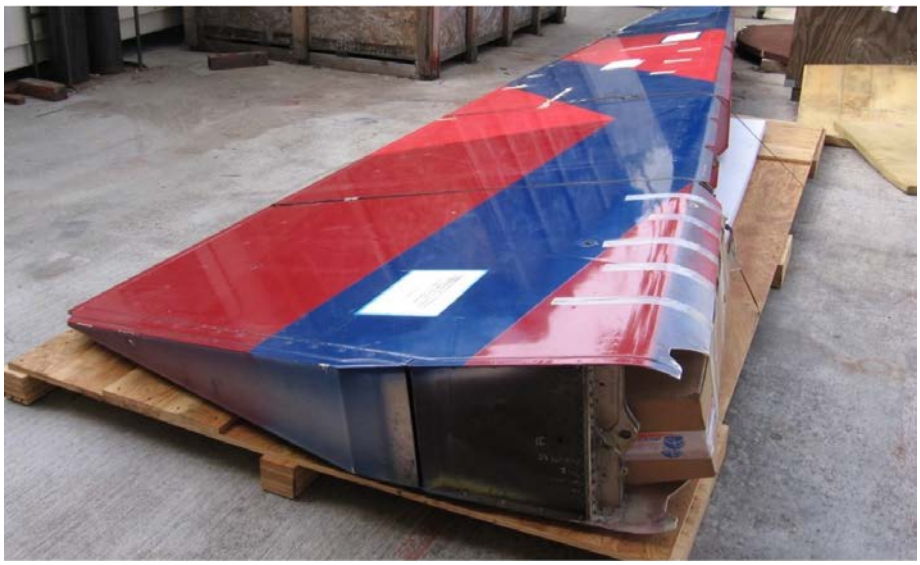

Figure 2.3.1. Airbus A320 rudder prior to sectioning.

305 mm wide by 710 mm tall panel specimens were cut from this rudder. Each panel could be impacted twice, once at the center of the top half and once at the center of the bottom half, allowing more tests to be achieved from the limited supply of test specimens. See Figure 2.3.2 to understand how the rudder section was divided. Each of the following measurements were averaged over ten points along a standard specimen. The front facesheet (impacted side of the panel) was 1.19 mm thick including the paint layer, and the back facesheet was 0.64 mm thick including the paint layer. Figure 2.3.3 shows where the wall-to-wall honeycomb cell size was measured and found to be 5.32 mm. The core thickness was 29.41 mm. Lastly, the core density was approximately 35 kg/m^3.

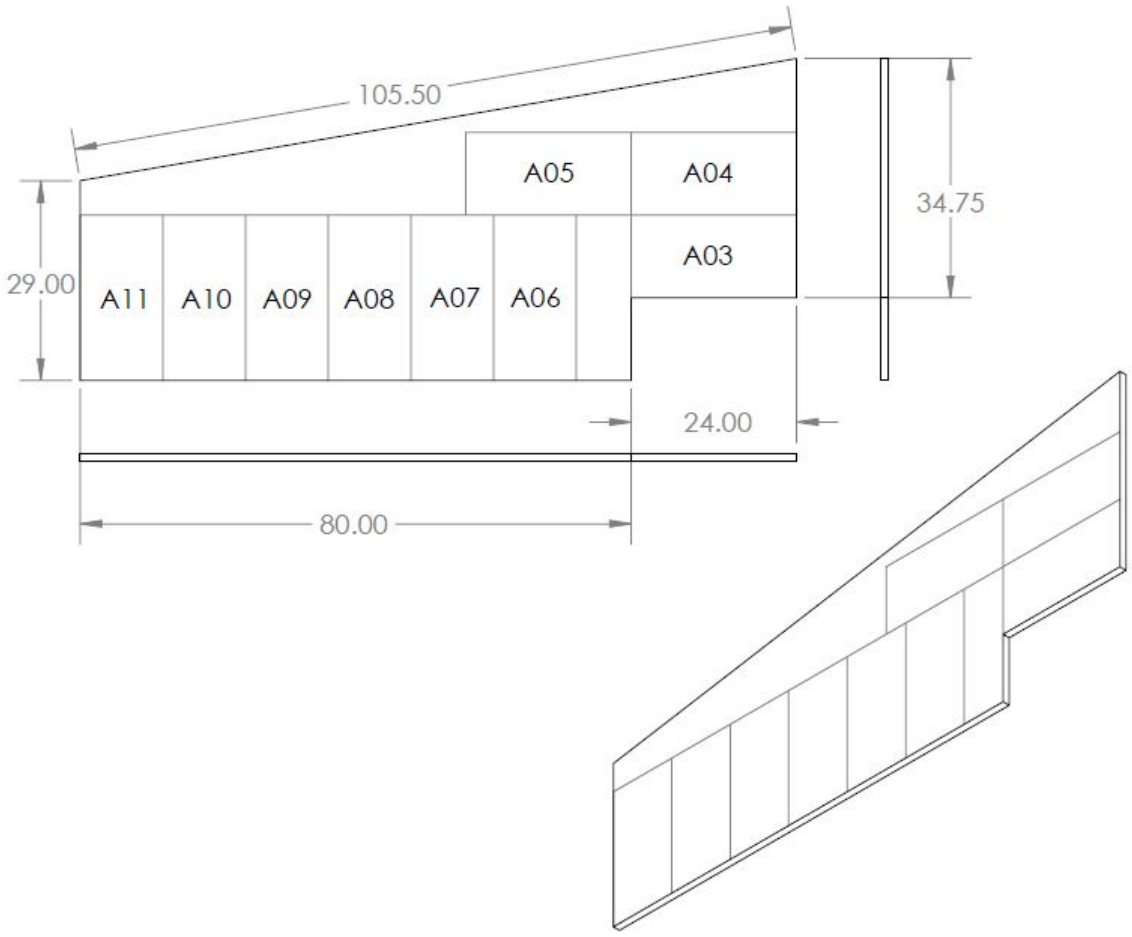

Figure 2.3.2. Distribution of test specimens from rudder section. Dimensions in inches.

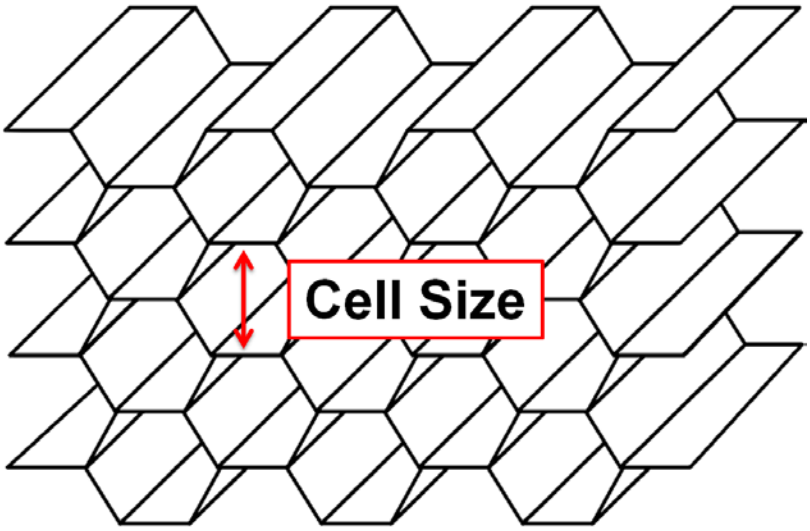

Figure 2.3.3. Ideally uniform geometry of honeycomb core.

The front and back facesheets had an inner layer of plain weave fiberglass, with an outer layer of a carbon fiber weave of [45º/-45º] orientation. However, certain parts of the rudder had an additional carbon fiber layer, resulting in an overall facesheet thickness of 1.87 mm. Since tests were conducted on specimens of both facesheet thicknesses, the single carbon fiber weave facesheet specimens will be referred to as “thin specimens” for the remainder of the study and the two-layer carbon fiber facesheet specimens will be referred to as “thick specimens”.

2.4 Test Equipment

The hail ice projectiles were fired through the high velocity gas gun at the University of California, San Diego (UCSD). This system consisted of multiple parts: a

pressurized tank where the propellant was stored prior to firing, the release mechanism which was a pressure-activated ball valve, a removable breech where the projectiles were loaded, a 2.29 m long barrel with an inner diameter of 79.3 mm, and a sabot stop plate that prevented the sabot from reaching the target. The gas gun can be seen in Figure 2.4.1. The tank contained the propellant gas, either helium or nitrogen, at pressures up to 1100 psi. Helium gas is used for firing projectiles at speeds of 200 m/s or greater, while the nitrogen gas is used at lower speeds of 150 m/s or less. The ball valve was actuated with a charge of helium gas, which released the main tank pressure in approximately 50 milliseconds. The propellant gas then traveled into the breech and expeled the projectile through the barrel and on to the target.

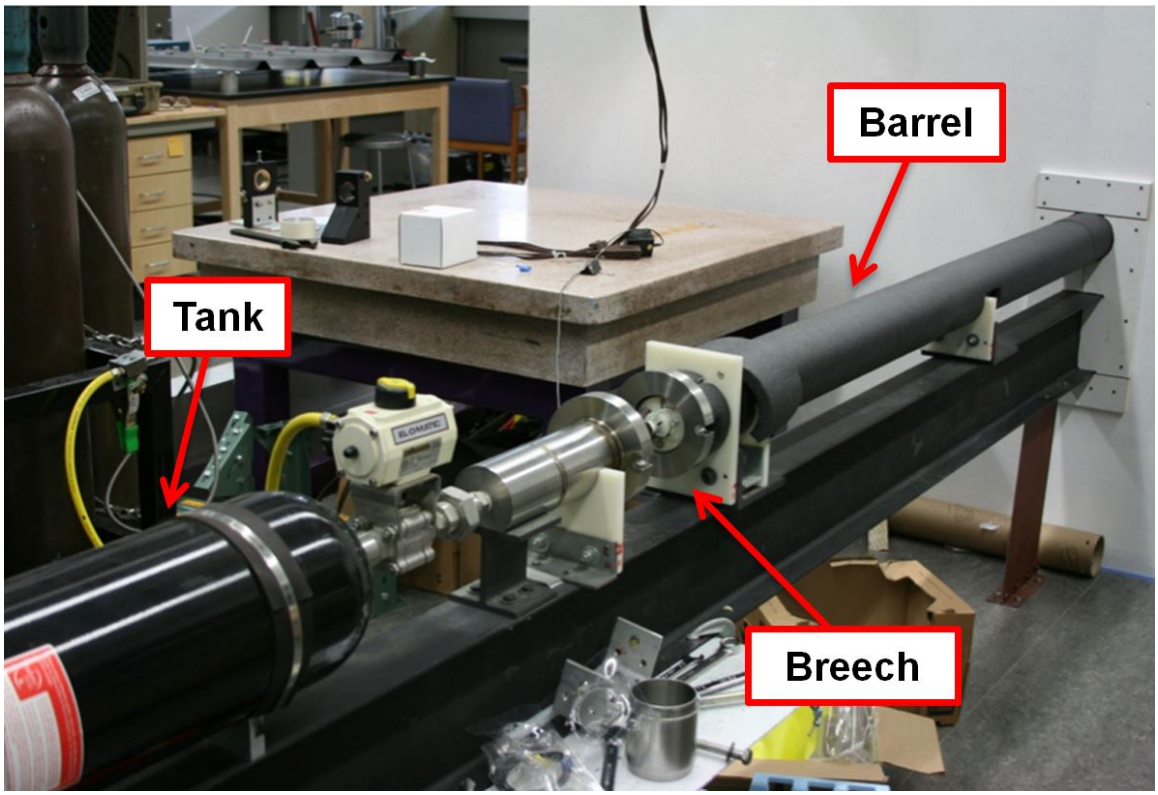

Figure 2.4.1. UCSD Gas Gun

The velocity of the projectile was then determined with a laser photogate system. The lasers were monitored with a 2-channel oscilloscope, and the lasers were spaced 0.1275 ± 0.0001 m apart. This system would measure the time when each laser was broken due to the projectile with a tolerance of ± 1.0%. From this information, it was possible to calculate the time, *t*, it took the projectile to pass through the photogate system. The unit housing this system can be seen in Figure 2.2.1. The velocity, *v*, of the hail ice projectile was calculated with this information using Equation 2.4.1 in base S.I. units.

$$v = \frac{0.1275}{t} \ (\mathrm{m/s}) \qquad \textbf{Equation 2.4.1}$$

Each test was documented with a Phantom v.7.3 high-speed camera at frame rates from 4,000 to 9,000 frames per second. This was necessary to confirm that the projectile arrived on-target and fully intact as there are times where defects within the hail ice projectile would cause it to break apart before contact with the target. The camera software also provided a method for measuring projectile velocity in case the laser photogate system failed.

The panels were held in a custom-built fixture using 80/20® T-slotted aluminum framing parts, as shown in Figure 2.4.2.

Figure 2.4.2. Panel-Holding Test Fixture.

The various parts of the fixture were held together with aluminum gusset plates, brackets, and 5/16-18 bolts with slide-in T-nuts. Through the use of brackets that could pivot and slide, the test angle was adjustable. The section that held the panel consisted of a picture-frame shaped steel fixture with a 571.5 x 266.7 mm opening that was attached to 76.2 mm long aluminum frame pieces. The frame halves were fixed in place with four Clutch Lock Bar Clamps (one at each corner). The surfaces of the frame that directly contacted the test specimens had a layer of 3.18 mm thick silicone rubber to protect the panels and reduce boundary-adjacent bending failures. Finally, the entire fixture was anchored into the ground with concrete anchors. An illustration of this test fixture in its multiple configurations can be seen in Figure 2.4.3.

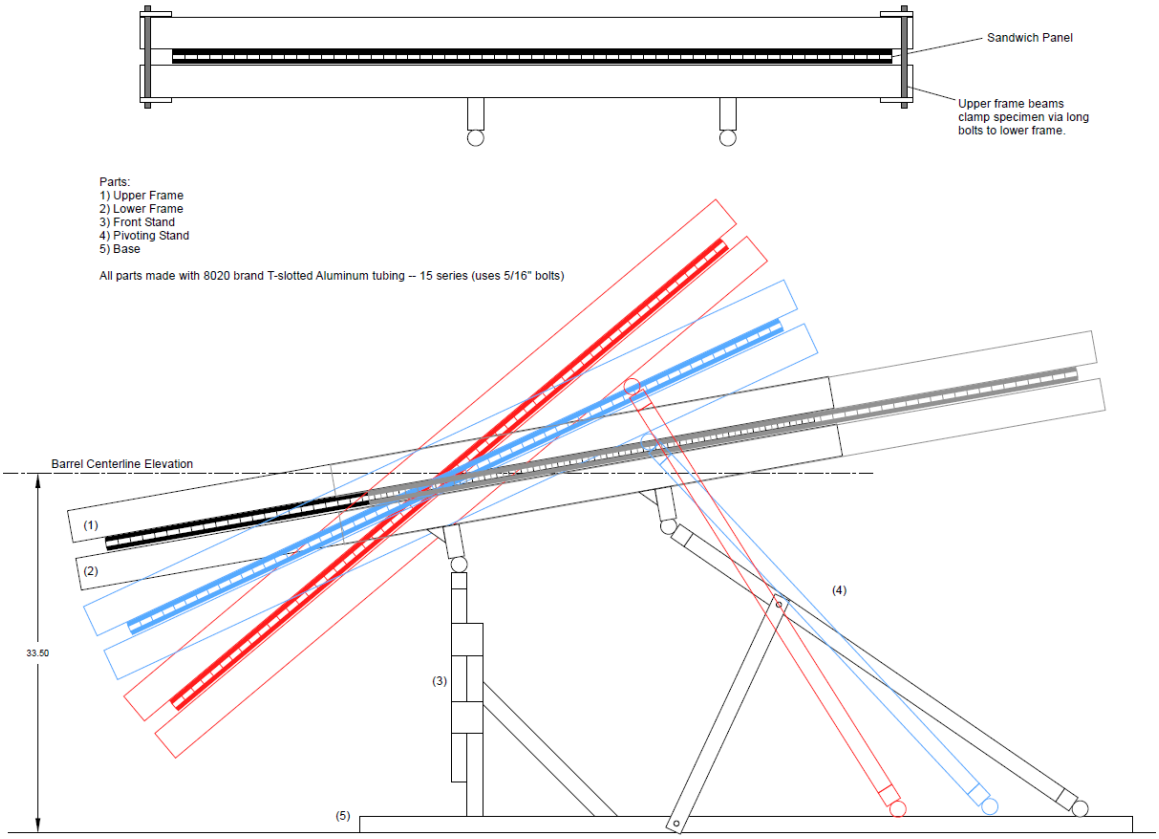

Figure 2.4.3. Preliminary Test Fixture Drawings

A digital protractor (PRO 3600 Digital Protractor) was utilized to determine the angle of the test fixture relative to the barrel's longitudinal axis. The protractor was placed on the surface of the frame while the fixture was adjusted as necessary and then fixed in place with bolts. The digital protractor is accurate to 0.1 degree.

A depth indicator (Mitutoyo Model ID-S1012E) was used to measure the dent depth at various points over the span of the impact site to create a dent depth profile. The depth indicator was mounted onto an 80/20 aluminum bar that was stiff enough to prevent the measurements from being affected by the handling of the tool. This system would slide along two precision ground bars that could be placed directly on the

specimen so that slight surface variations would be minimized. The system was used to measure the depth at fixed intervals that are marked prior to testing, and the data was directly recorded into an excel file. The measurements using this system were quite sensitive and a high level of noise in the data was attributed to various human factors (distribution of force on the bar, amount of force used in holding the bar down) as well as variations in the materials themselves. Therefore, in order to minimize inconsistency, three scans were always conducted just prior to testing as well as after testing. The average profile of the pre-scans would be subtracted from the average of the post-scans, providing the final dent depth profile.

A digital weight scale (Ohaus Scout Pro SP 2001) was used to weigh the mass of the sabot and the combined mass of the sabot with the hail ice projectile. The mass of the hail ice was calculated from the difference of the two. The scale had a tolerance of ± 0.1 grams.

In order to minimize variables in the testing conditions, a stopwatch was always used to aim to fire the projectile at 3:00 minutes after removal from the freezer. This was to reduce the number of unknown factors that could cause the ice to fail prior to impact and to ensure that the temperature of the hail ice would be the same for every test.

2.5 Testing Procedure

Prior to testing, the test fixture was adjusted to the desired test angle. The test panel was marked at 10 mm intervals spanning from +80 mm to -80 mm with 0 being the

target location. Next, the pre-test surface profile was measured three times. Then, the test site was labeled with the test number and placed into the fixture. The laser photogate system was turned on and connected to the computer and the lights were oriented to shine the maximum amount of light on the target panel. The high-speed camera was set up to capture the view of the panel as well as the trajectory of the projectile before impact. Finally, all the necessary programs were calibrated to record the velocity and the video footage.

The masses of the sabot and hail ice projectile were then recorded and they were immediately loaded into the front end of the barrel and pushed in three feet as shown in Figure 2.5.1. This was found to improve the consistency of the velocity and the structural integrity of the hail ice projectile for the low velocities used in these tests (all less than 55 m/s).

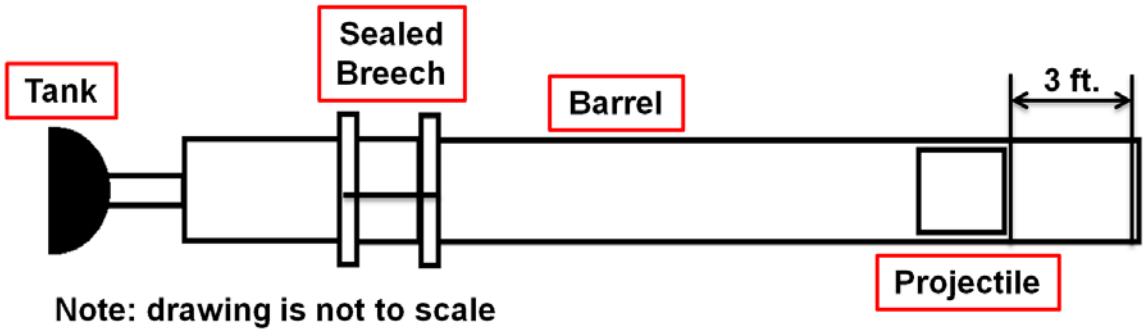

Figure 2.5.1. Front-loaded projectile ready to be fired.

The breech was then sealed and bolted tight, the gas gun was pressurized to the necessary pressure levels, and the projectile was fired at the 3:00 minute mark. If this was the first test of the day, then multiple test shots would be fired into a bucket for

calibration purposes because the conditions of the projectile fit, weight, and pressure levels resulted in variability in the corresponding velocity. Previous tests would be used to estimate the starting point, and actual testing would begin when three shots within ± 5% of the desired velocity were achieved consecutively.

After the test was completed, the video footage and the picoscope data were recorded and the test specimen was removed and cleaned off to measure the dent depth profile. Once all necessary measurements were taken, the panel was then longitudinally sectioned in order to visually inspect the internal state of the core.

2.6 Data Collection

During each impact test, the SHI would pass through the laser photogate system seen in Figure 2.2.1. The voltage information was saved on the computer through the PicoScope data acquisition system. An example of the data is shown in Figure 2.6.1 which represents a successful test where the SHI was fired without any issues and reached the target fully intact. The blue line represents the first laser, while the red line represents the second laser. As the SHI passed through the first laser, the voltage incrased to approximately 3.6 V and then quickly dropped off after nearly 1 ms. Then, after a total of 2.340 ms, the SHI passed through the second laser, which caused the voltage to rise to 3.6 V again. The time of flight information was then combined with the known distance between the two lasers and the SHI mass to calculate the velocity and kinetic energy using Equation 2.4.1 and Equation 3.1.1.

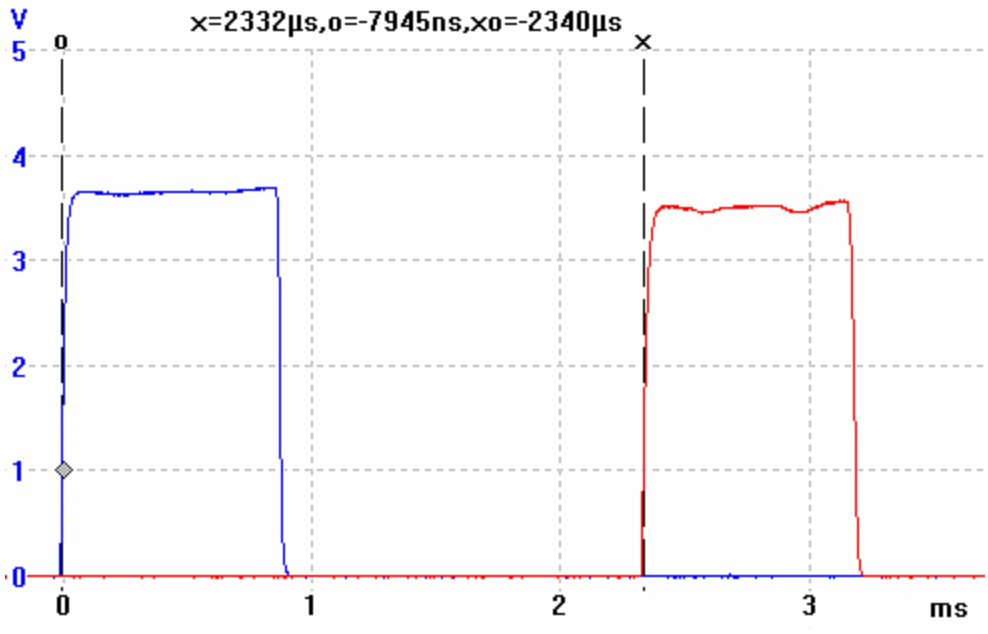

Figure 2.6.1. PicoScope data for Test-046 (54.49 m/s at 40 degrees).

Sometimes the PicoScope did not trigger properly for unknown reasons, and the video was then used to find a rough estimate of the SHI velocity. One example of a failed test is Test-045, where there is no velocity information because the SHI disintegrated due to the flaws in the ice and high gas pressure. This is observed in Figure 2.6.2, which shows the first laser not triggering properly, and the second laser was entirely evaded. Because the ice broke apart, it was not possible to obtain a rough estimate of the speed using the video, but since the ice did not impart much energy onto the panel, this information was not necessary.

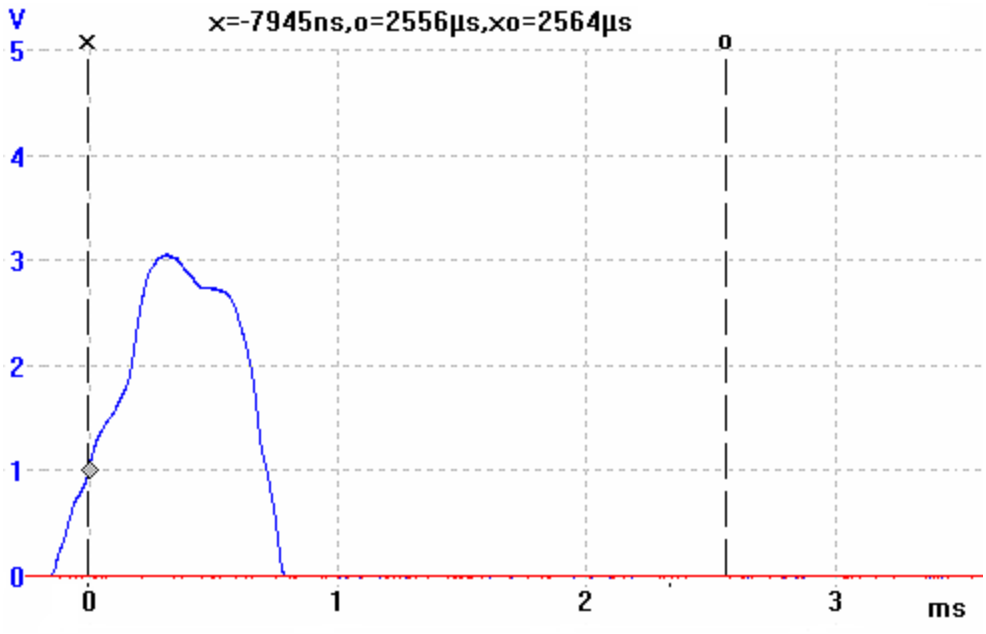

Figure 2.6.2. PicoScope data for Test-045.

3 RESULTS

3.1 SUMMARY

During the course of the study, 18 hail ice impact tests were conducted using 10 thin carbon/epoxy facesheet honeycomb sandwich panels and 8 thick sandwich panels at nominal speeds of 25 m/s and 50 m/s and incidence angles of 25, 40, and 90 degrees (90 being normal impact). The peak dent depth information is summarized along with the impact parameters for all the tests in Table 3.1.1 and Table 3.1.2. “Mass” in the tables refers to the mass of the SHI. “KE” refers to the kinetic energy of the SHI prior to impact, which was calculated with the recorded mass and velocity using Equation 3.1.1.

$$KE = \frac{1}{2}mv^2 \text{ (J)} \qquad \textbf{Equation 3.1.1}$$

The tests are organized by test angle and the test numbers are non-consecutive because these tables do not include all the velocity calibration tests.

Table 3.1.1. Summary of peak dent depth for thin specimens.

Test Angle (^{0})	Panel ID	Test NO.	Velocity (m/s)	Mass (g)	KE (J)	Visible Dmg. (Y/N)	Peak Dent (mm)
90	A01	001	24.23	61.9	18.17	Y	0.64
90	A01	002	47.63	61.6	69.88	Y	Penetrated
40	A02	005	23.67	59.4	16.63	Y	0.53
40	A02	003	24.69	60.6	18.47	Y	0.64
40	A02	004	32.03	60.1	30.83	Y	0.92
40	A02	006	44.76	58.9	58.99	Y	Penetrated
25	A03	008	23.90	61.0	17.42	N	0.04
25	A04	017	28.02	61.4	24.11	Y	0.07
25	A03	015	43.31	65.8	61.72	Y	0.44
25	A06	041	54.10	61.2	89.56	Y	Penetrated

Table 3.1.2. Summary of peak dent depth for thick specimens.

Test Angle (^{0})	Panel ID	Test NO.	Velocity (m/s)	Mass (g)	KE (J)	Visible Dmg. (Y/N)	Peak Dent (mm)
25	A05	029	25.07	61.3	19.26	N	0.01
25	A05	032	49.38	61.7	75.24	Y	0.02
25	A06	036	51.81	61.9	83.09	Y	0.16
25	A04	018	48.26	65.4	76.17	Y	0.35
40	A07	045	-	60.5	-	N	0.00
40	A08	052	23.15	59.5	15.94	N	0.02
40	A08	051	25.46	63.1	20.45	N	0.03
40	A07	046	54.49	61.9	91.90	Y	Penetrated

Many of the impacts did not leave any noticeable dent or damage, however, the trials may have still been identified as showing visible damage if distortions of the oblique reflected lighting could be seen on the surface of the panel due to very slight

changes in surface curvature. This method of identifying surface damage required knowledge of the impact location as well as very close scrutiny of that location and under specific lighting conditions. In reality, this would not be a reliable method of detecting damage because many impact events may go unnoticed or the location may not be obvious; i.e., when inspecting a large aircraft for damage one would most likely not find such shallow dents.

The main focus of the tests conducted in this study was to identify what possible modes of damage could realistically occur under these varying impact parameters. To do so, the dent profile of each test was measured, and the peak dent was extracted from that information. In addition, the specimens were bisectioned length-wise through the impact zone as shown in Figure 3.1.1 to allow for direct observation of the internal damage modes and extent. The internal damage state was then related to the impact test conditions and externally-observed dent depth.

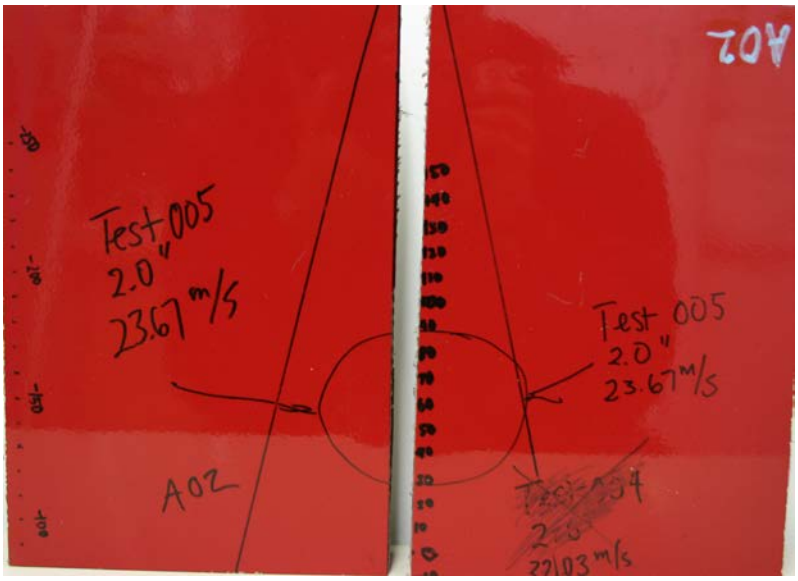

Figure 3.1.1. Bisection through impact zone of Test-005 on Panel A02.

Figure 3.1.2 plots the information presented in Table 3.1.1. The three points that are located on the horizontal axes are impact tests that penetrated the facesheet, so no dent measurements were taken. These results indicate an expected trend where increasing levels of energy produce increasing levels of dent. In addition, steeper angles require smaller amounts of energy to produce higher levels of dent.

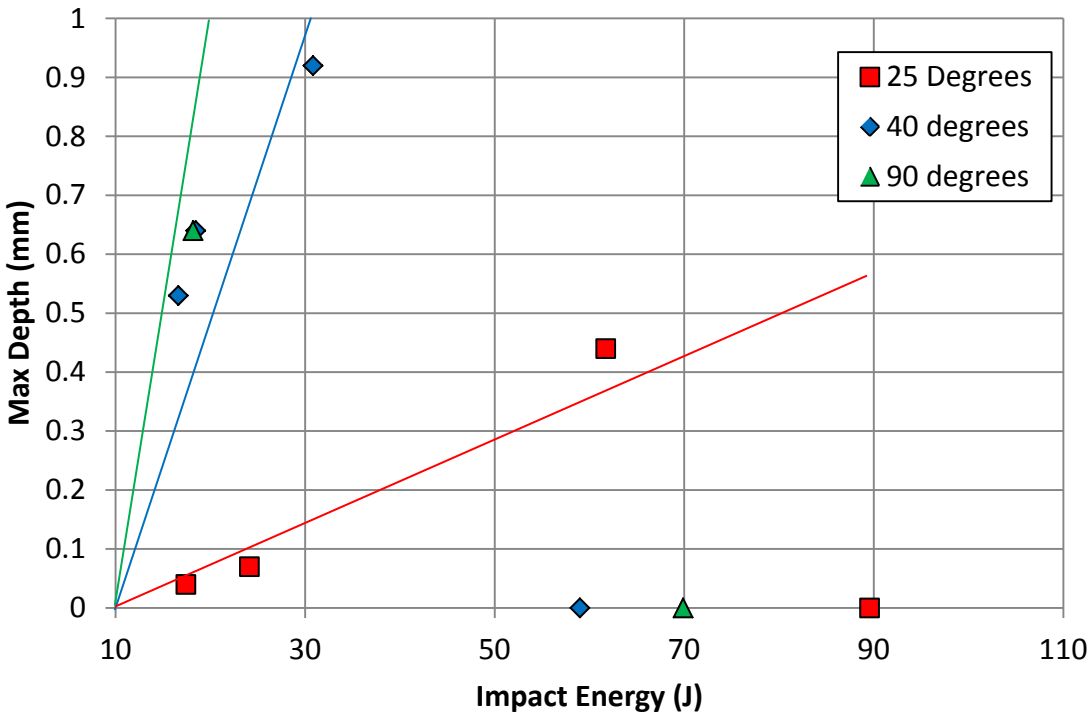

Figure 3.1.2. Relationship between impact energy and peak dent depth for thin facesheet specimens.

The behavior of the thick facesheet specimens was not as predictable, as seen in Figure 3.1.3. For these specimens, there is not a clear correlation between impact energy and peak dent depth, but the results seem to suggest that the steeper angle tests require more energy to produce greater levels of dent (which should not be the case). The cause

for this phenomenon is most likely due to the status of ice upon impact and is further explained in the discussion section of this thesis.

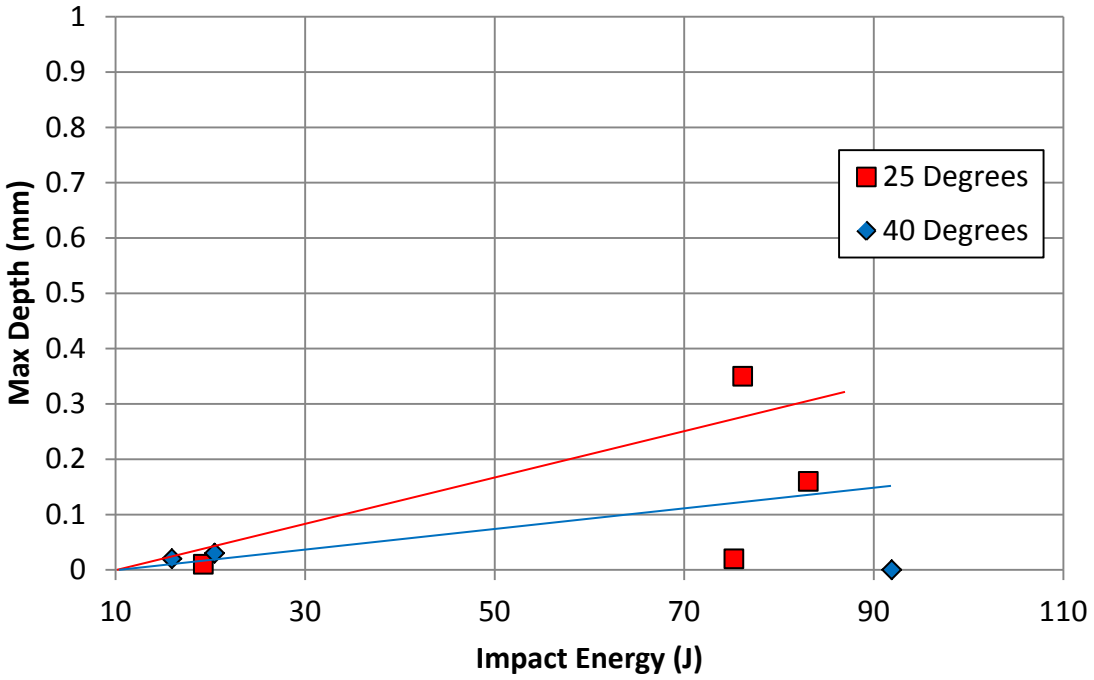

Figure 3.1.3. Relationship between impact energy and peak dent depth for thick facesheet specimens.

In Figure 3.1.4, the peak dent depth of every impact test was plotted against the normal impact energy calculated using the normal component of the impact velocity with Equation 3.1.1 in order to determine the existence of a relationship, but none was found.

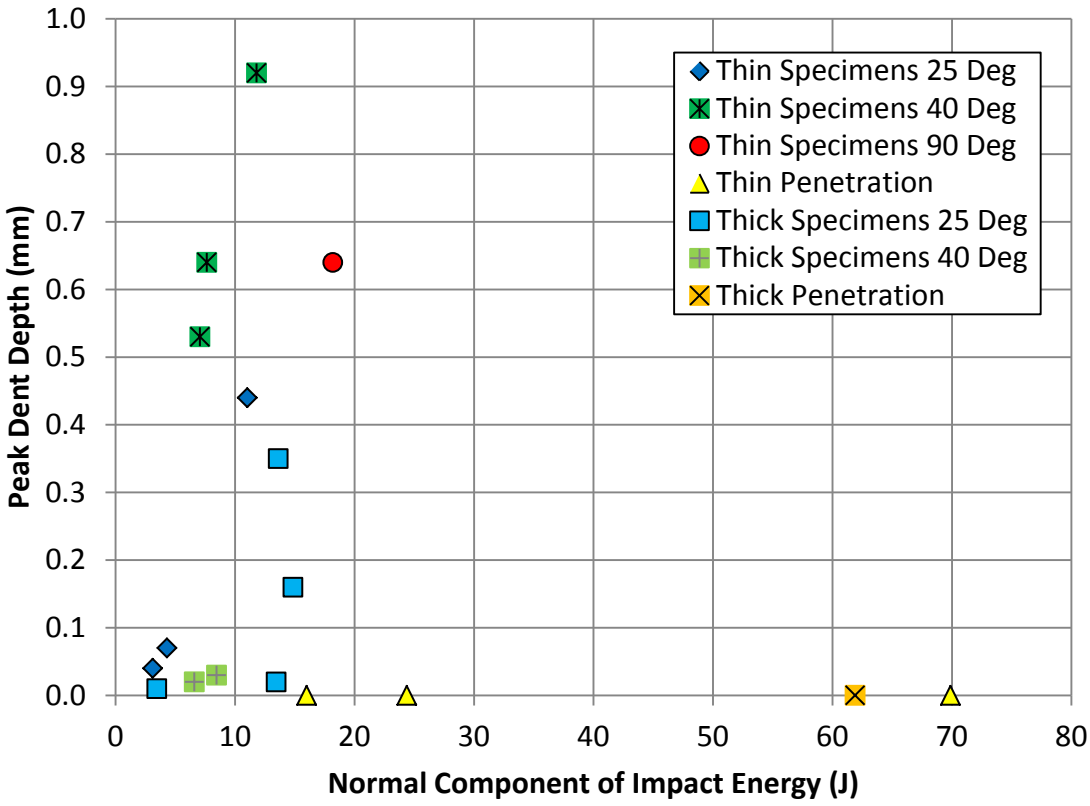

Figure 3.1.4. All peak dents plotted against normal component of impact energy.

3.2 Dent Depth Profile

After each impact test, the panel was removed from the fixture so the dent depth profile could be measured. Initially, measurements were taken every 10 mm starting 100 mm above the target, through the center, and ending 100 mm below the target. This provided a visual profile of the impact zone, and the peak dent (if any) was extracted from this information. Some of the specimens had a splice running horizontally through them, so they had an upper portion with a thick facesheet and a lower portion with a thin

facesheet. Because this distribution was not even (usually 2/3 of the panel consisted of thick facesheet material), it was not possible to have a test site spanning from +100 mm to -100 mm with a single facesheet thickness. As a result, the span was reduced to +80 mm to -80 mm, and in one case, +70 mm to -70 mm. This did not affect the results because the deformations were very localized around the target site.

There were five different types of damage modes identified: A) no visible or measurable dent without core damage, B) no visible but measurable damage with core damage, C) visible and measurable dent with significant core damage, D) facesheet penetration, and E) no visible or measurable damage with core damage. An example of a Mode A profile can be seen in Figure 3.2.1. There is no discernable dent from the profile and no detectable defects in the surface.

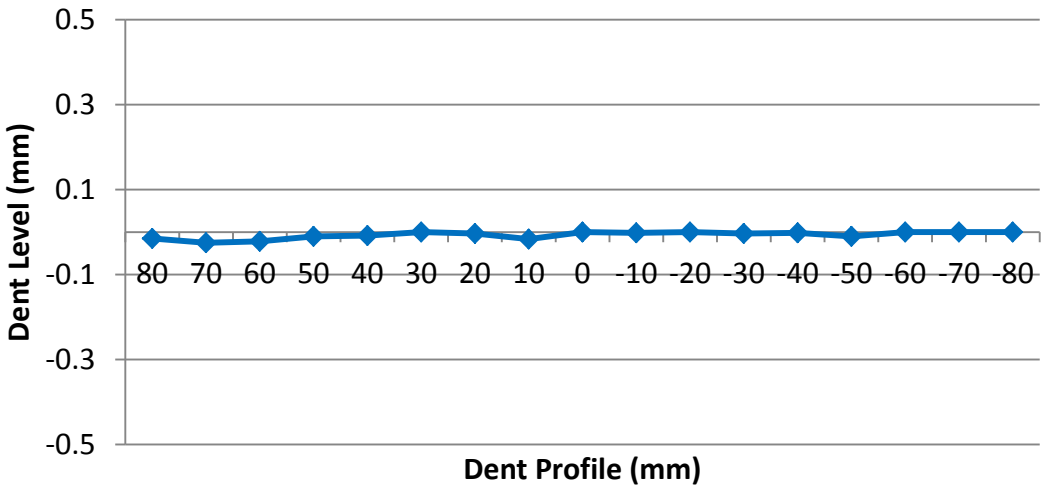

Figure 3.2.1. Dent profile of Test-052 on thick facesheet Panel A08 (23.14 m/s at 40 degrees).

Figure 3.2.2 features Mode B damage where the impact did not leave a readily visible dent, but there was a measurable dent of 0.04 mm at the point of impact around -40 mm.

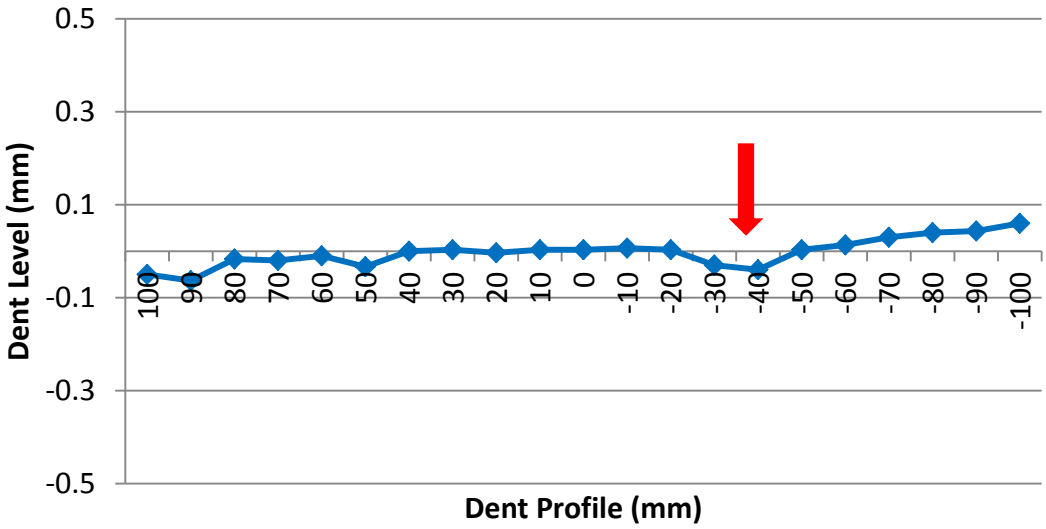

Figure 3.2.2. Dent profile of Test-008 on thin facesheet Panel A03 (23.90 m/s at 25 degrees).

Mode C can be seen in Figure 3.2.3 and Figure 3.2.4 where there is an easily visible dent on the surface highlighted by the yellow circle as well as a clearly defined dent profile.

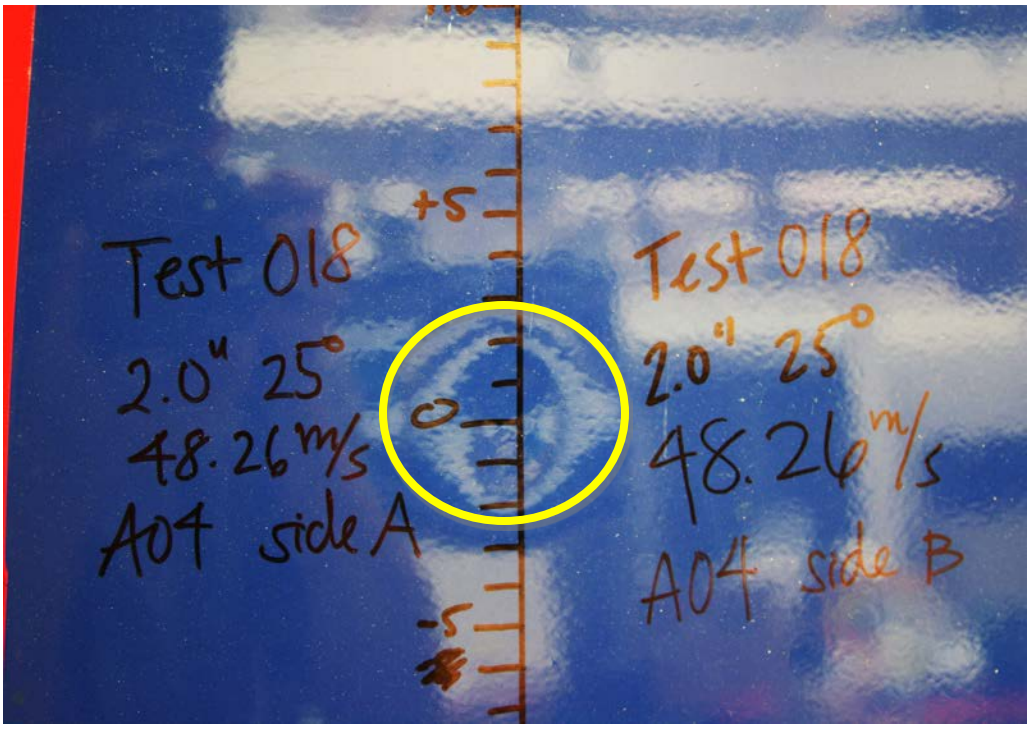

Figure 3.2.3. Visible dent from Test-018 on thick facesheet Panel 04.

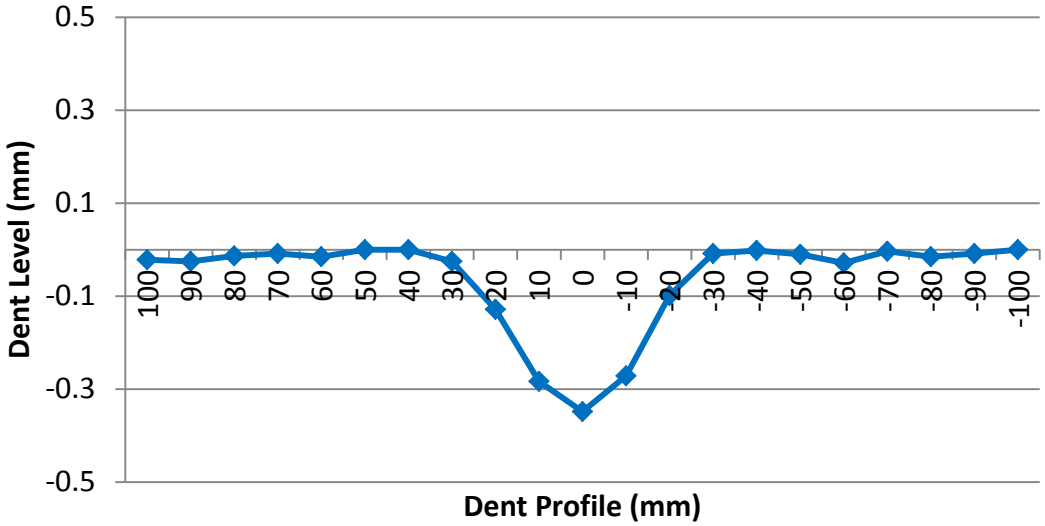

Figure 3.2.4. Dent profile of Test-018 on thick facesheet Panel 04 (48.26 m/s at 25 degrees).

Mode D can be seen in Figure 3.2.5; a dent profile was not created for Test-006 because the facesheet was penetrated.

Figure 3.2.5. Visible skin penetration from Test-006 on thin facesheet Panel A02 (40 degrees).

At first glance, Figure 3.2.6 appears to be a Mode A case where there is no visual/measurable damage, perhaps suggesting that there is no internal damage (such as in Figure 3.2.1). However, after destructive sectioning is performed, it is clear that there is significant core damage and the case actually represents Mode E. Therefore, visual inspections and even procedures conducted on the surface are not necessarily reliable metrics to determine the presence of internal damage.

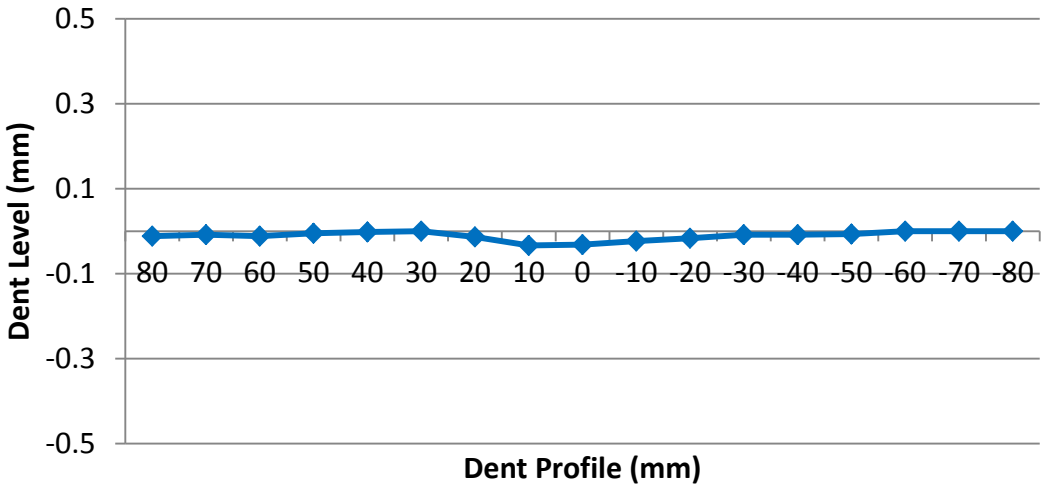

Figure 3.2.6. Dent profile of Test-051 on thick facesheet Panel A08 (25.46 m/s at 40 degrees).

3.3 Destructive Sectioning

Once a panel had been thoroughly examined and all necessary measurements were taken, it would then be longitudinally sectioned down the mid-line of impact zone. Destructive sectioning of all the thin facesheet specimens revealed that all of them had varying degrees of core damage which can be organized into three modes: I) slight cell wall wrinkling, II) cell wall buckling, III) core fracture. The thin facesheet specimens were impacted at 25 degrees, 40 degrees, and 90 degrees, at both 25 m/s and 50 m/s (nominal speeds), and the 50 m/s impacts consistently produced facesheet penetration at every test angle. Mode I core damage was only present in the 25 degree impact tests at 25 m/s. Figure 3.3.1 shows a thin facesheet specimen that exhibits Mode I core damage.

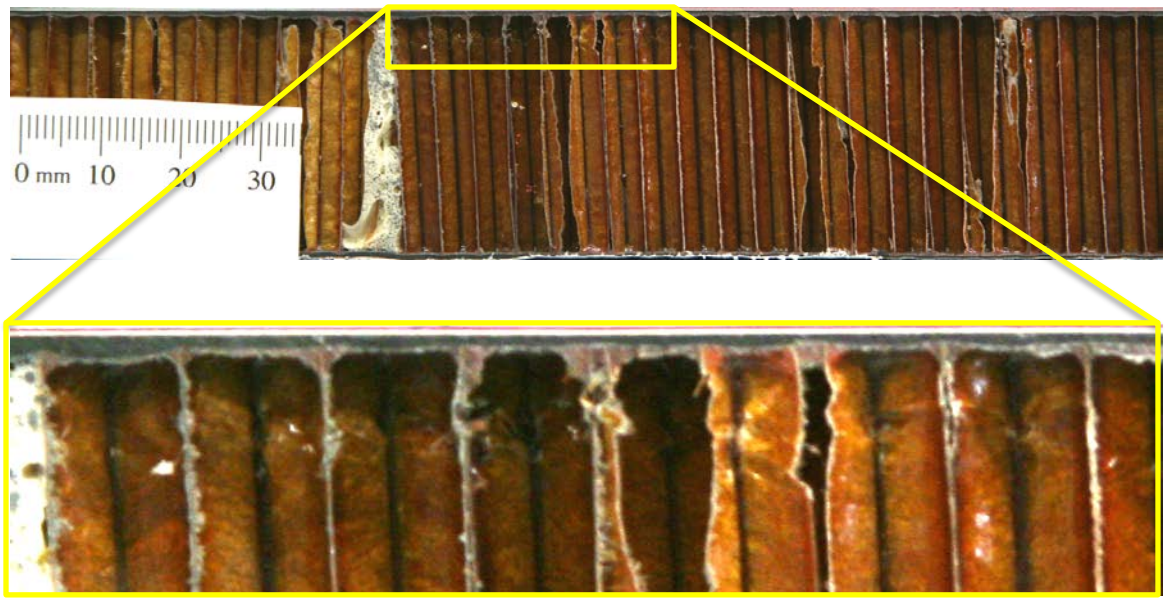

Figure 3.3.1. Mode I core damage in Test-017 on thin facesheet Panel A04 (28.02 m/s at 25 degrees, 0.07 mm peak dent).

Mode II core damage is distinguished by more pronounced folds in the cell wall structure. The span of core damage is nearly twice as long as usual in Figure 3.3.2 because two impact tests (Test-003 and Test-004) took place in that region. This occurred when the SHI fired slower than predicted due to a significant amount of pressure leaking out of the gas gun prior to firing. The result was that the SHI exited the barrel at a lower speed and struck the panel beneath the target, ending up next to the previous impact zone. For thin facesheets, Mode II core damage only occurred in the 40 degree impact tests at the 25 m/s speed, whereas the 50 m/s test penetrated the outer facesheet.

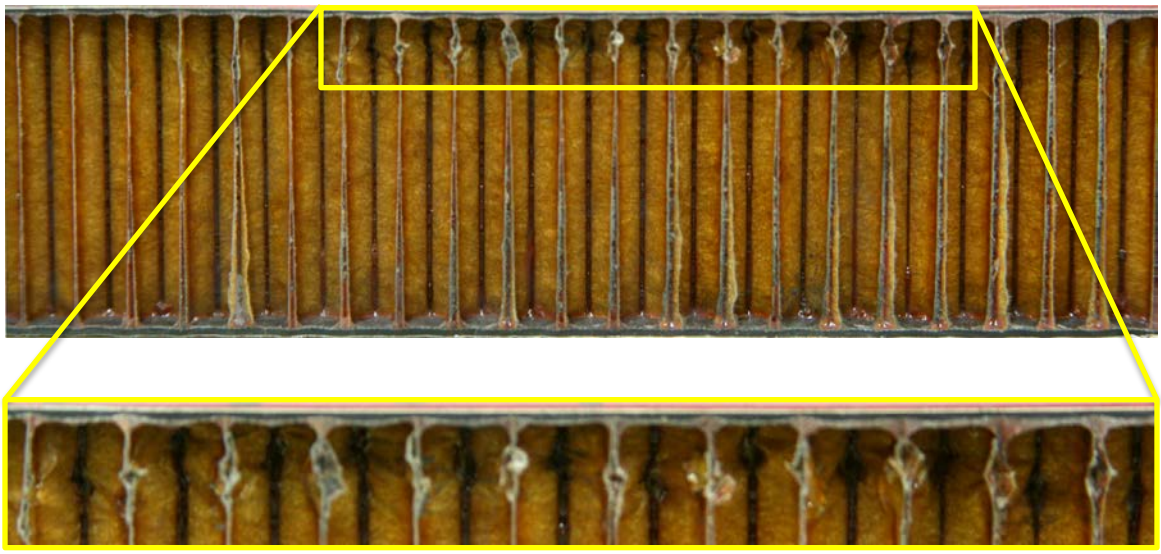

Figure 3.3.2. Mode II core damage in Test-003 on thin facesheet Panel A02 (24.69 m/s at 40 degrees, 0.64 mm peak dent).

Mode III core damage is different from the previous two damage modes in that the cell walls actually fractured in addition to wrinkling. For the thin facesheet specimens, this damage mode only occurred in one test at 25 degrees and 50 m/s. This scarcity is likely because this damage mode represents a more local event that requires a higher velocity impact without penetrating the facesheet (otherwise the penetration would result in a lot of core buckling, but not fracture). Significant core fracture damage can be seen in Figure 3.3.3.

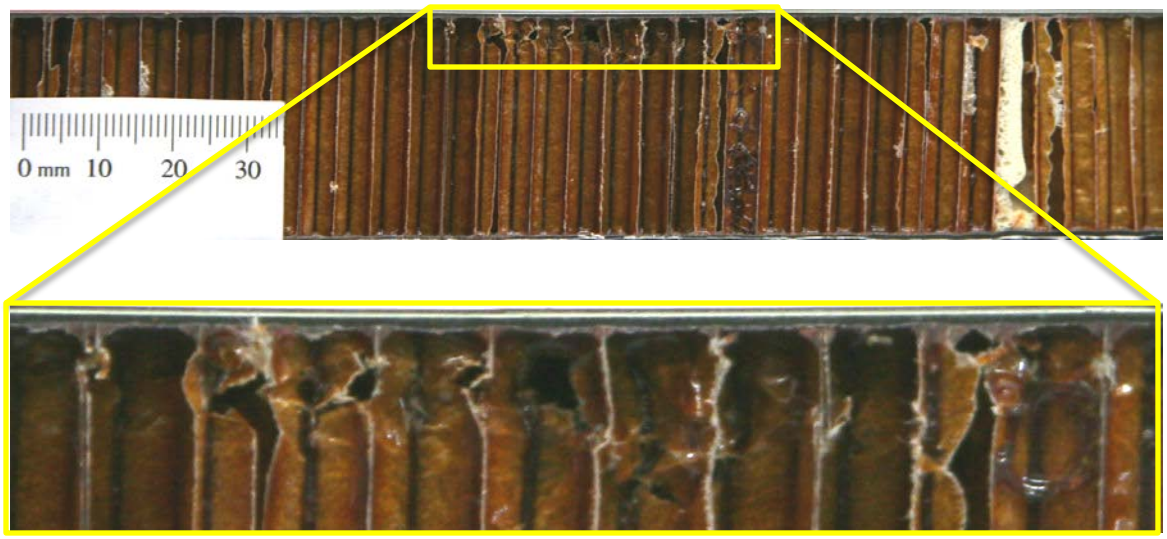

Figure 3.3.3. Mode III core damage in Test-015 on thin facesheet Panel A03 (43.31 m/s at 25 degrees, 0.44 mm peak dent).

The thick facesheet specimens behaved quite differently from the thin facesheet specimens. These specimens were only impacted at 25 degrees and 40 degrees at 25 and 50 m/s. The results were inconsistent and not quite predictable: out of three 25 degree tests at 50 m/s, two exhibited Mode III damage while one barely showed any sign of Mode I wrinkling. Out of two 40 degree tests at 25 m/s, one exhibited Mode III damage while the other had no evidence of damage. These results show that Mode III damage can occur at varying levels of energy. Figure 3.3.4 shows very pronounced core fracture that was caused by a high 89.56 J energy impact, while Figure 3.3.5 shows that similar damage can be produced by a low 20.45 J energy impact.

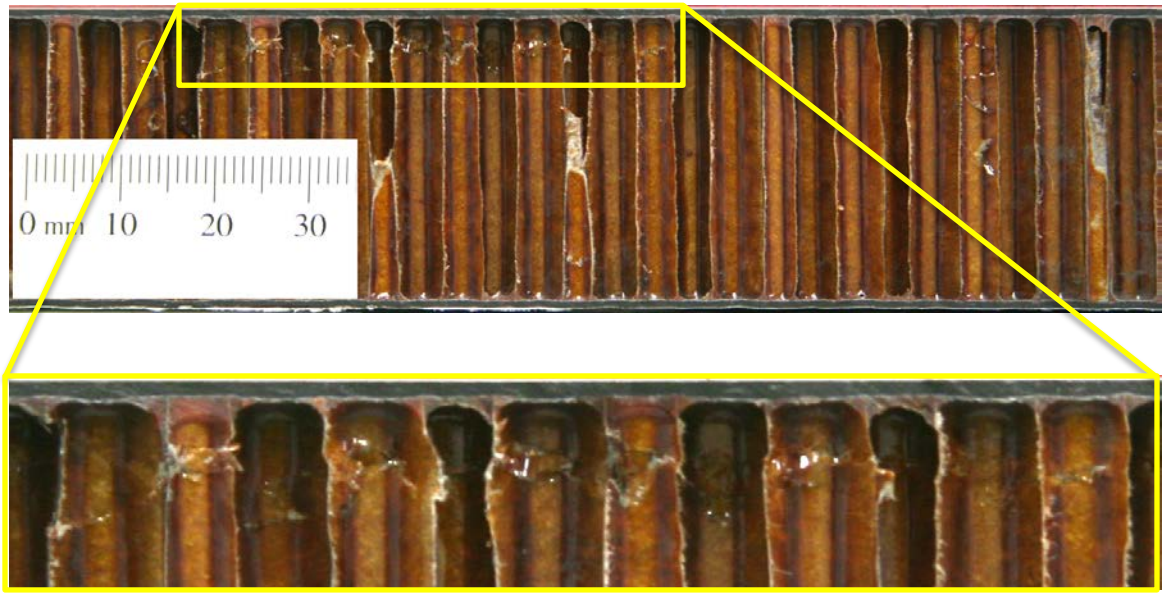

Figure 3.3.4. Mode III core damage in Test-036 on thick facesheet Panel A06 (51.81 m/s at 25 degrees, 0.16 mm peak dent).

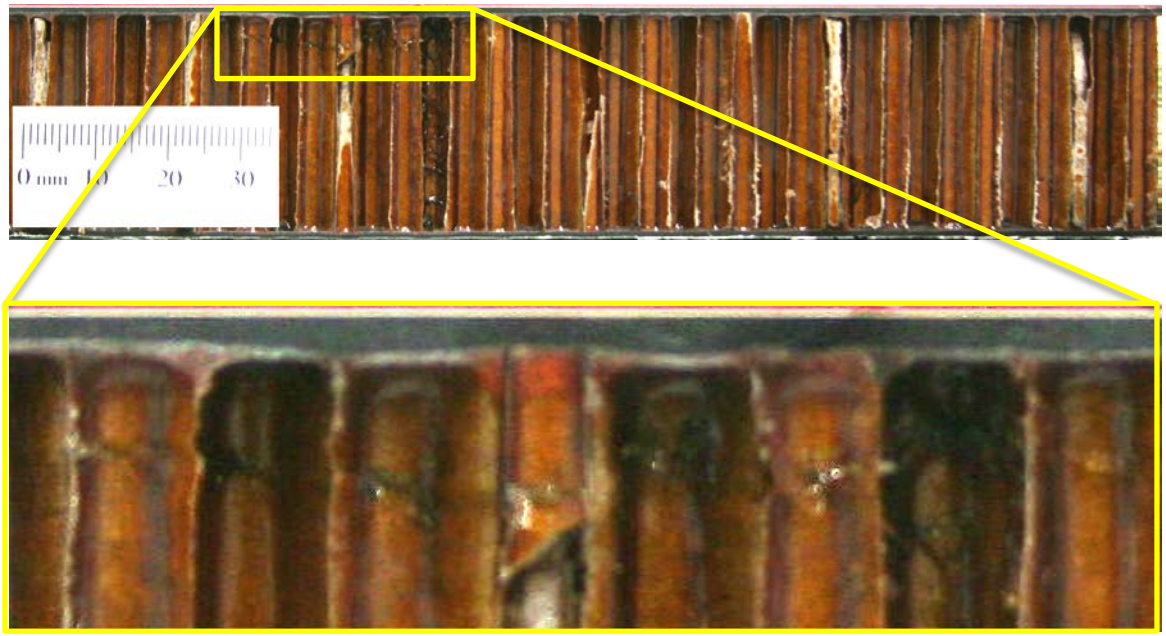

Figure 3.3.5. Mode III core damage in Test-051 on thick facesheet Panel A08 (25.46 m/s at 40 degrees, 0.03 mm peak dent).

All types of core damage consistently occurred at 3-5 mm of depth, regardless of the facesheet thickness or testing parameters. It is probable that the high velocities in this study resulted in a highly localized impact phenomenon.

4 DISCUSSION AND CONCLUSIONS

Composite sandwich materials are being used more frequently in the aircraft industry because of their favorable structural properties. They can be stiffer and stronger than their traditional metallic counterparts yet are also very lightweight. The drawback is that their response to impact loads is not well understood, particularly high velocity hail ice impact. These impact events have been found to result in damage that is not readily visible but could grow and lead to large-scale failure through the repetitive loading cycles of aircraft. It is necessary to gain more knowledge on composite sandwich materials in order to increase their usage while maintaining a high standard of safety. Furthermore, hail ice and bird impact damage costs the worldwide aircraft industry billions of dollars each year, so it is important from an economic standpoint to improve the understanding of impact damage response of composite sandwich structures.

The experimental study described in this thesis investigated the effect of high velocity simulated hail ice impact on composite sandwich panels of two facesheet thicknesses (1.19 mm and 1.87 mm). The test specimens were impacted at angles of 25, 40, and 90 degrees at nominal speeds of 25 and 50 m/s with energy levels ranging from 15.94 to 91.90 J. The dent depth profiles of each specimen were recorded to characterize the resulting damage state. Then, the specimens were longitudinally sectioned to reveal the internal damage state.

These tests revealed that the thin facesheet specimens behaved as expected: higher energies and steeper impact angles would result in larger dents. However, the thick facesheet specimens did not behave as predictably; on several occasions, similar energy impacts would result in largely different dent level responses. Ultimately, destructive sectioning revealed that in all specimens, when surface damage was visually detectable or measurable, there would be some existing level of core damage. However, the converse was not true; there were cases where core damage was present without any measurable level of damage on the surface. This was particularly frequent in the thick facesheet specimens. There were several cases with no visible dent and peak dents of at most 0.03 mm, but significant Mode III core fracture present. There was also a case where two impacts of 15-20 J and dent responses of 0.02-0.03 mm had different internal responses: one exhibited Mode III damage while the other had no core damage. This indicates that the traditional method of visual damage inspection is not reliable for composite sandwich structures. A lack of visible dent may imply a lack of internal damage, but often times there may be significant levels of core fracture hidden. The inconsistent results in the thick facesheet specimens are likely due to the status of the ice upon impact. Due to the stiffer facesheets, the ice would often break apart upon impact and lose a lot of energy in that process, as opposed to striking the target and transferring all the energy into the core.

A relationship between impact energy levels and internal damage state was not found. Test-036 had an impact energy of 83 J and a peak dent of 0.16 mm, so Mode III core fracture was present as expected. However, Test-051 and Test-052 had impact

energies of 20.5 and 16 J and peak dents of 0.03 and 0.02 mm, respectively, yet Test-051 also exhibited Mode III core fracture while Test-052 did not have core damage. However, there was a slight correlation between impact angles and resulting damage states. For the thin facesheet specimen, 25 degree impacts produced Mode I wrinkling at 25 m/s and Mode III fracture at 50 m/s, while 40 degree impacts all produced Mode II buckling (even when the facesheet was penetrated). At the velocities investigated, the core damage tended to be a highly localized phenomenon where the depth of core damage was consistently independent of impact angle or energy.

Now that a foundation has been formed in identifying the possible damage states arising from realistic hail ice impact conditions, future work could be geared towards improving the understanding of the residual effects of these damage states. Various residual strength tests could be conducted to explore the possible reduction in strength, if any. This information could lead into improvements in analytical models, and models that are more accurate would benefit the airline industry by reducing the necessity for costly and time-consuming destructive testing. The formation of hail ice is also a complex process that often results in oddly shaped projectiles that may have different impact characteristics, so a more extensive study on hail ice projectiles may also improve the understanding of its threat and the resulting damage created to this lightweight composite sandwich.

5 REFERENCES

[1] B. Roeseler, B. Sarh, and M. Kismarton, “Composite Structures – The First 100 Years,” in *16th International Conference on Composite Materials*, Kyoto, pp. 1-41, July 2007.

[2] A. Arias, J. Lopez-Puente, J. Antonio Loya, D. Varas, and R. Zaera, "Analysis of High-Speed Impact Problems in the Aircraft Industry", *Constitutive Relations Under Impact Loadings*, vol. 552, pp. 137-207, 2014.

[3] A. S. Herrmann, P. C. Zahlen, and I. Zuardy, “Sandwich Structures Technology in Commercial Aviation: Present Applications and Future Trends,” *Sandwich Structures: Advancing with Sandwich Structures and Materials*, vol. 7, pp. 13–26, 2005.

[4] F. A. Amir, A. R. Othman, and H. M. Akil, “Damage Characterization of Polypropylene Honeycomb Sandwich Panels Subjected to Low-Velocity Impact,” *Advances in Materials Sciene and Engineering*, vol. 2013, pp. 1–10, 2013.

[5] J. Pernas-Sanchez, D. A. Pedroche, D. Varas, J. Lopez-Puente, and R. Zaera, “Numerical modeling of ice behavior under high velocity impacts,” *International Journal of Solids and Structures*, vol. 49, no. 14, pp. 1919–1927, 2012.

[6] T. D. McQuigg, R. K. Kapania, S. J. Scotti, and S. P. Walker, “Compression After Impact Experiments on Thin Face Sheet Honeycomb Core Sandwich Panels,” *Journal of Spacecraft and Rockets*, vol. 51, no. 1, pp. 253–266, 2014.

[7] R. Hilgers, “Substantiation of Damage Growth within Sandwich Structures,” in *FAA Workshop for Composite Damage Tolerance and Maintenance*, Tokyo, pp. 1–47, June 2009.

[8] S. Sistek. “Nebraska Homes, Cars Blasted By Tennis Ball-Sized Hail,” http://www.komonews.com/weather/blogs/scott/Incredible-rain-hail-storm-blasts-Nebraska-261862201.html, Jun. 4, 2014 [Jul. 22, 2014].

[9] M. Alves, C. E. Chaves, and R. S. Birch, “Impact on aircraft,” in *17th International Congress of Mechanical Engineering*, São Paulo, pp. 1–8, 2003.

[10] A. R. Othman and D. C. Barton, “Failure Initiation and Propagation Characteristics of Honeycomb Sandwich Composites,” *Composite Structures*, vol. 85, no. 2, pp. 126–138, 2008.

[11] T. Anderson and E. Madenci, “Experimental Investigation of Low-Velocity Impact Characteristics of Sandwich Composites,” *Composite Structures*, vol. 50, no. 3, pp. 239–247, 2000.

[12] K. S. Raju, B. L. Smith, J. S. Tomblin, K. H. Liew, and J. C. Guarddon, “Impact Damage Resistance and Tolerance of Honeycomb Core Sandwich Panels,” *Journal of Composite Materials*, vol. 42, no. 4, pp. 385–412, 2008.

[13] H. Kim, D. A. Welch, and K. T. Kedward, “Experimental Investigation of High Velocity Ice Impacts on Woven Carbon/Epoxy Composite Panels,” *Composites Part A: Applied Science and Manufacturing*, vol. 34, pp. 25–41, 2003.

[14] J. Rhymer, H. Kim, and D. Roach, “The Damage Resistance of Quasi-Isotropic Carbon/Epoxy Composite Tape Laminates Impacted by High Velocity Ice,” *Composites Part A: Applied Science and Manufacturing*, vol. 43, no. 7, pp. 1134–1144, 2012.

[15] J. M. Swift, “Simulated Hail Ice Mechanical Properties and Failure Mechanism at Quasi-Static Strain Rates,” M.S. Thesis, Department of Aeronautics and Astronautics, University of Washington, Seattle, WA, 2013.

[16] ASTM Standard F320-10, 2005 (2010), “Standard Test Method for Hail Imapct Resistance of Aerospace Transparent Enclosures,” *ASTM International*, West Chonshohocken, PA, 2010, DOI: 10.1520/F0320-10, www.astm.org

[17] C. Q. Sun, “Mpemba Paradox: H-Bond Memory and Skin Supersolidity,” in *Relaxation of the Chemical Bond*, vol. 108, pp. 763–774, 2014.

APPENDIX A. RAW DATA TABLES

UCSD 2013 Ice Impact Test Data Sheets

Test No.	Date	Target ID	Facesheet Type	Angle (deg)	Gun Press., psi	Ice Dia. in.	Sabot Mass, g	Sabot + Ice Mass, g	Ice Mass*, g	Laser Brk Time, msec	Veloc.*, m/s	KE (J)	Time Frz to Fire m:ss	Notes	Visible Dmg (Y/N)	Max Dent Depth (mm)	Residual Dent Depth (mm)
001	2/5/2013	A01	Thin	90.0	30.3	2	66.9	128.8	61.9	5.263	24.23	18.17	3:00	Sabot loaded 1 foot deep, projectile fractured	Y		~0.64
002	2/5/2013	A01	Thin	90.0	74.6	2	56.4	118.0	61.6	2.677	47.63	69.88	4:00	loaded 1 foot deep, panel cratered	Y	cratered	-
003	2/19/2013	A02	Thin	40.0	30.0	2	68.0	128.6	60.6	5.164	24.69	18.47	5:00	loaded 1 foot deep, no video	Y	~0.64	~0.63
004	2/19/2013	A02	Thin	40.0	49.9	2	67.6	127.7	60.1	3.981	32.03	30.83	3:00	shot hit panel below target	Y	~0.90	~0.92
005	2/28/2013	A02	Thin	40.0	33.2	2	70.0	129.4	59.4	5.388	23.67	16.63	4:00		Y	~0.53	~0.56
006	2/28/2013	A02	Thin	40.0	79.6	2	67.2	126.1	58.9	2.849	44.76	58.99	3:00	panel cratered	Y	cratered	-
007	9/25/2013	bucket	-	25.0	35.0	2	58.9	120.0	61.1	5.237	24.35	18.11	3:00	loaded from front of barrel 1 ft	-	-	-
008	9/26/2013	A03	Thin	25.0	35.0	2	60.5	121.5	61.0	5.336	23.90	17.42	3:00	loaded from front of barrel 1 ft	N	0.033	
009	11/6/2013	bucket	-	25.0	85.0	2	65.0	126.3	61.3	4.050	31.48	30.38	3:00	loaded from front of barrel 1 ft	-	-	-
010	11/6/2013	bucket	-	25.0	85.0	2	63.8	127.0	63.2	3.955	32.24	32.85	3:00	loaded from front of barrel 1 ft	-	-	-
011	11/6/2013	bucket	-	25.0	100.0	2	60.8	123.4	62.6	3.570	35.72	39.93	3:00	loaded from front of barrel 1 ft	-	-	-
012	11/8/2013	bucket	-	25.0	120.0	2	61.0	126.7	65.7	-	-	-	3:00	loaded from front of barrel 1 ft; ice broke before laser	-	-	-
013	11/8/2013	bucket	-	25.0	90.0	2	66.0	131.7	65.7	2.594	49.16	79.38	3:00	loaded from front of barrel 3 ft; successful	-	-	-
014	11/11/2013	bucket	-	25.0	90.0	2	59.9	124.0	64.1	2.656	48.01	73.87	3:00	from this point on loaded 3 ft from front	-	-	-
015	11/11/2013	A03	Thin	25.0	90.0	2	58.1	123.9	65.8	2.944	43.31	61.72	3:00		Y	0.395	
016	11/12/2013	bucket	-	25.0	32.0	2	56.7	122.6	65.9	5.889	21.65	15.45	3:00		-	-	-
017	11/12/2013	A04	Thin	25.0	30.0	2	55.5	116.9	61.4	4.550	28.02	24.11	3:00		Y	0.023	-
018	11/12/2013	A04	Thick	25.0	90.0	2	55.2	120.6	65.4	2.642	48.26	76.17	3:00		Y	0.35	-
019	12/19/2013	bucket	-	25.0	40.0	2	65.3	126.8	61.5	3.747	34.03	35.61	3:00		-	-	-
020	12/19/2013	bucket	-	25.0	35.0	2	64.2	129.4	65.2	4.240	30.07	29.48	3:00		-	-	-
021	12/19/2013	bucket	-	25.0	30.0	2	63.1	126.6	63.5	6.882	18.53	10.90	3:00		-	-	-
022	12/19/2013	bucket	-	25.0	30.0	2	62.9	127.8	64.9	6.476	19.69	12.58	3:00		-	-	-
023	1/24/2014	bucket	-	25.0	35.0	2	62.2	123.6	61.4	4.274	29.83	27.32	3:00		-	-	-
024	1/24/2014	bucket	-	25.0	32.0	2	61.4	122.8	61.4	4.473	28.51	24.95	3:00		-	-	-
025	1/25/2014	bucket	-	25.0	28.0	2	60.6	122.7	62.1	-	-	-	3:00		-	-	-
026	2/5/2014	bucket	-	25.0	25.0	2	58.4	118.5	60.1	5.086	25.07	18.89	3:00	normal fit	-	-	-

UCSD 2013 Ice Impact Test Data Sheets

Test No.	Date	Target ID	Facesheet Type	Angle (deg)	Gun Press., psi	Ice Dia, in	Sabot Mass, g	Sabot + Ice Mass, g	Ice Mass*, g	Laser Brk Time, msec	Veloc.*, m/s	KE (J)	Time Frz to Fire m:ss	Notes	Visible Dmg. (Y/N)	Max Dent Depth (mm)	Residual Dent Depth (mm)
027	2/5/2014	bucket	-	25.0	30.0	2	58.2	121.0	62.8	5.656	22.54	15.96	3:00	tight fit	-	-	-
028	2/5/2014	bucket	-	25.0	28.0	2	57.6	119.3	61.7	5.371	23.74	17.39	3:00	medium-tight fit	-	-	-
029	2/5/2014	A05	Thick	25.0	25.0	2	56.6	117.9	61.3	5.086	25.07	19.26	3:00	normal fit; no video	N	0.007	-
030	2/7/2014	bucket	-	25.0	80.0	2	57.2	118.2	61.0	2.616	48.74	72.46	3:00	loose fit	-	-	-
031	2/7/2014	bucket	-	25.0	88.0	2	59.6	120.0	60.4	2.599	49.06	72.69	3:00	normal fit	-	-	-
032	2/7/2014	A05	Thick	25.0	85.0	2	57.5	119.2	61.7	2.582	49.38	75.24	3:00	loose-normal fit	N	0.012	-
033	2/18/2014	bucket	-	25.0	85.0	2	56.0	116.1	60.1	2.677	47.63	68.18	3:00	normal fit	-	-	-
034	2/18/2014	bucket	-	25.0	88	2	54.6	115.1	60.5	2.633	48.43	70.94	3:00	normal fit	-	-	-
035	2/18/2014	bucket	-	25.0	90	2	52.4	114.2	61.8	2.720	46.88	67.91	3:00	tight fit	-	-	-
036	2/18/2014	A06	Thick	25.0	95	2	61.9	123.8	61.9	2.461	51.81	83.09	3:00	normal fit; ice cracked on impact	-	-	-
037	2/20/2014	bucket	-	25.0	95	2	63.7	124.8	61.1	2.694	47.33	68.44	3:00	normal fit	-	-	-
038	2/20/2014	bucket	-	25.0	95	2	61.5	123.3	61.8	2.823	45.17	63.04	3:00	medium-tight fit; ice broke before impact	-	-	-
039	2/20/2014	bucket	-	25.0	85	2	58.4	118.0	59.6	2.841	44.88	60.03	3:00	loose-normal fit	-	-	-
040	2/20/2014	bucket	-	25.0	101	2	59.7	119.8	60.1	2.452	52.00	81.26	3:00	medium-tight fit	-	-	-
041	2/20/2014	A06	Thin	25.0	100	2	63.7	124.9	61.2	2.357	54.10	89.56	3:00	normal fit	Y	fractured	-
042	2/21/2014	bucket	-	25.0	95	2	60.3	123.1	62.8	2.651	48.10	72.64	3:00	normal fit	-	-	-
043	2/21/2014	bucket	-	25.0	95	2	59.3	120.6	61.3	2.461	51.81	82.28	3:00	loose-normal fit	-	-	-
044	2/21/2014	bucket	-	25.0	95	2	58.6	121.3	62.7	2.564	49.73	77.53	3:00	normal fit	-	-	-
045	2/21/2014	A07	Thick	40.0	95	2	61.5	122.0	60.5	-	-	-	3:00	loose-normal fit; ice crushed before impact	-	-	-
046	2/21/2014	A07	Thick	40.0	100	2	61.9	123.8	61.9	2.340	54.49	91.90	3:00	loose-normal fit; panel cratered	Y	cratered	-
047	2/21/2014	bucket	-	40.0	27	2	55.3	117.6	62.3	6.778	18.81	11.02	3:00	medium-tight fit	-	-	-
048	2/21/2014	bucket	-	40.0	35	2	54.8	117.4	62.6	3.903	32.67	33.41	3:00	normal fit	-	-	-
049	2/21/2014	bucket	-	40.0	29	2	54.6	113.6	59.0	5.250	24.29	17.40	3:00	medium-tight fit	-	-	-
050	2/21/2014	bucket	-	40.0	31	2	53.7	116.2	62.5	5.397	23.63	17.44	3:00	medium-tight fit	-	-	-
051	2/21/2014	A08	Thick	40.0	32	2	53.3	116.4	63.1	5.008	25.46	20.45	3:00	medium-tight fit; ice cracked on impact	N	0.008	-
052	2/21/2014	A08	Thick	40.0	30	2	52.6	112.1	59.5	5.509	23.15	15.94	3:00	normal fit; ice cracked on impact	N	0.022	-

APPENDIX B. SURFACE DENT SCANS

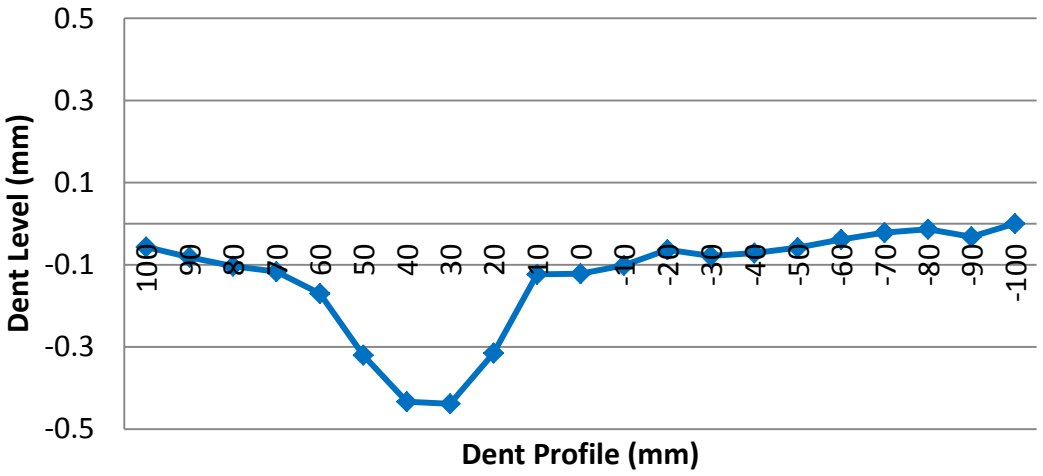

Test-015 of thin facesheet Panel A03 (43.31 m/s at 25 degrees)

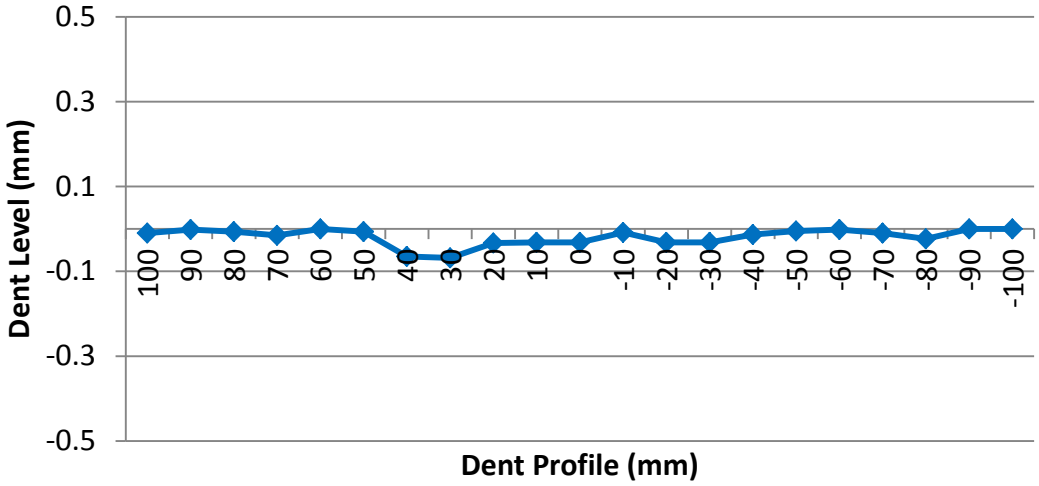

Test-017 on thin facesheet Panel A04 (28.02 m/s at 25 degrees)

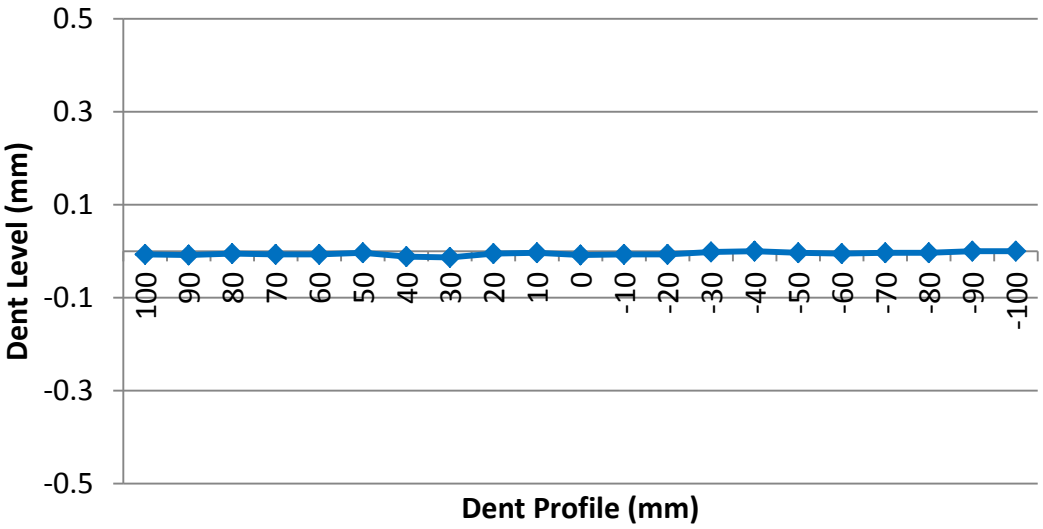

Test-029 on thick facesheet Panel A05 (25.07 m/s at 25 degrees)

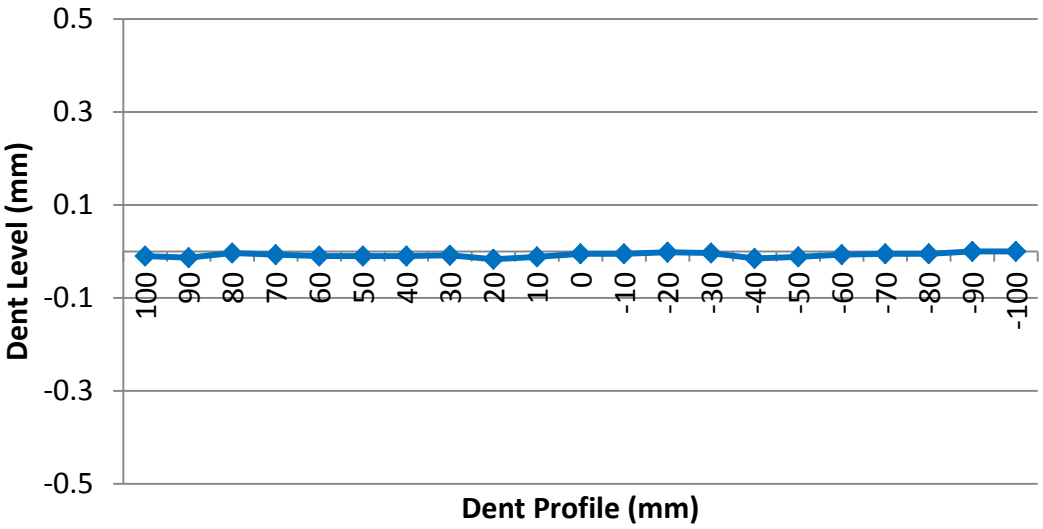

Test-032 on thick facesheet Panel A05 (49.38 m/s at 25 degrees)

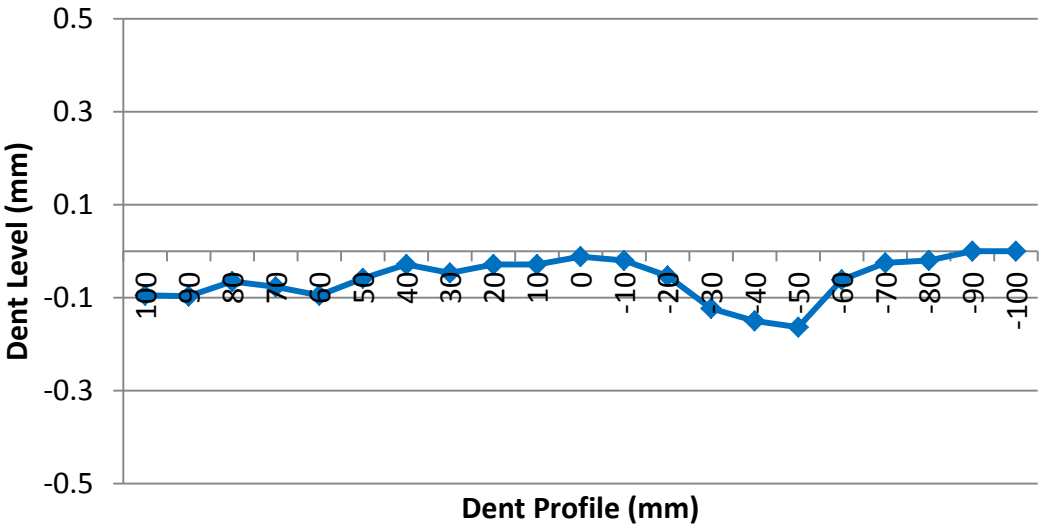

Test-036 on thick facesheet Panel A06 (51.81 m/s at 25 degrees)

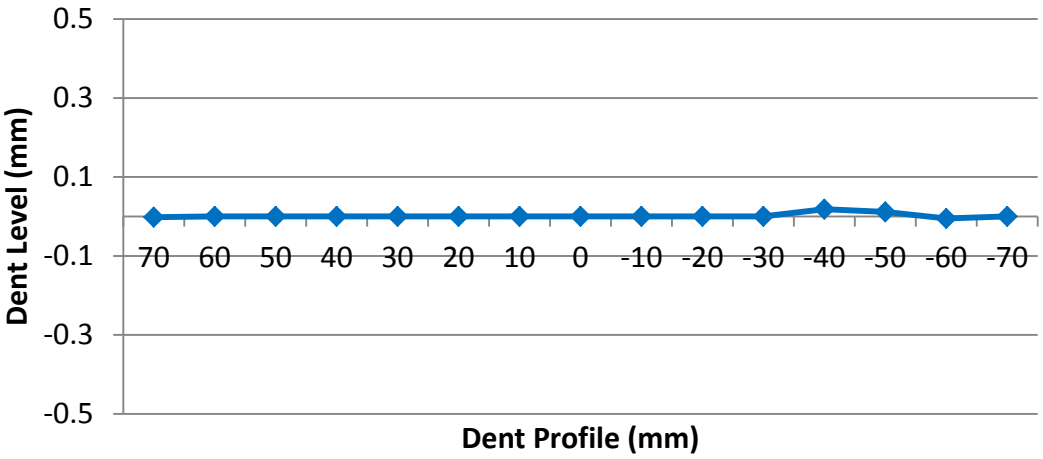

Test-045 on thick facesheet Panel A07 (speed unknown at 40 degrees)

APPENDIX C. CORE DAMAGE PHOTOS

Peak dent 0.53 mm, Test-005 on thin facesheet Panel A05 (23.67 m/s at 40 degrees), visible dent with Mode II core buckling

Peak dent 0.04 mm, Test-008 on thin facesheet Panel A03 (23.90 m/s at 25 degrees), no visible dent with Mode I core wrinkling

Peak dent 0.07 mm, Test-017 on thin facesheet Panel A04 (28.02 m/s at 25 degrees), no visible dent with Mode I core wrinkling

Peak dent 0.35 mm, Test-018 on thick facesheet Panel A04 (48.26 m/s at 25 degrees), ice cracked, slid and then reflected off the panel, visible dent with Mode III core fracture

Peak dent 0.01 mm, Test-029 on thick facesheet Panel A05 (25.07 m/s at 25 degrees), status of ice upon impact unknown, no visible dent

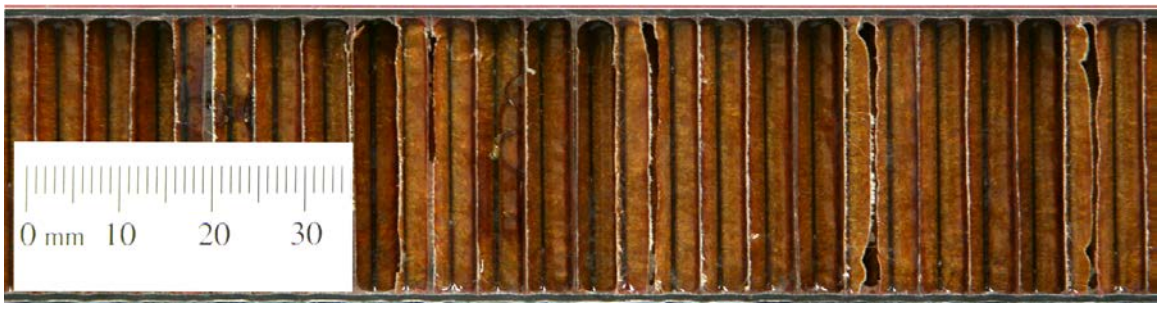

Peak dent 0.02 mm, Test-032 on thick facesheet Panel A05 (49.38 m/s at 25 degrees), ice broke prior to impact, very slightly noticeable dent, minor Mode I core wrinkle

Peak dent 0, Test-045 on thick facesheet Panel A07 (speed unknown at 40 degrees), ice crushed before impact, no visible dent, no core damage

Peak dent 0.02 mm, Test-052 on thick facesheet Panel A08 (23.15 m/s at 40 degrees), ice broke up on impact, no visible dent, no core damage

APPENDIX D. STEP BY STEP ICE FABRICATION PROCEDURE

1. Clean entire surface of both halves of the ice mold using alcohol.
2. Apply mold release to all the hemispherical surfaces of the ice mold.
3. Carefully apply petroleum jelly around the circumference of each hemispherical cavity of the top half of the ice mold (the half that contains the fill holes). Use enough to form a complete seal, but make sure not to get any in the hemispherical cavity.
4. Boil deionized water for at least 5 minutes.
5. Pour boiling hot deionized water into the appropriate cavities in bottom half of the mold.
6. Place the other half of the mold on top and secure in place using the pegs.
7. Use c-clamps to thoroughly secure both mold halves together.
8. Use syringes to fill the rest of the mold with boiling hot deionized water until it overflows.
9. Remove excess off the top surface of the mold.
10. Draw out precalculated amount of water from the fill hole so that the mass of water in the mold is the same as the final desired ice mass. Be sure to include the volume of the fill hole channel in the subtracted volume amount. For the 2.0 in. diameter ice molds used in this research, 5 mL was extracted from each cavity.
11. Immediately place mold in freezer (below 5° F) for at least 6 hours.

12. Upon removal, run c-clamps under water for approximately 30 seconds (or however long is necessary) until the clamps are warm enough to remove.
13. Carefully separate molds apart slightly with a screwdriver or similar tool, and then pull off the top half of the mold with both hands so that no moment is exerted on the SHI.
14. Take the half of the mold with the SHI still frozen in the cavities and run the bottom half under a small stream of running water for approximately 5-10 seconds (or however long is necessary).
    a. Make sure not to wet the SHI.
    b. Do not run the water for too long and cause the SHI to melt too much.
15. Remove SHI as soon as possible and quickly transfer to a sealed plastic bag and place it in the freezer for storage.

APPENDIX E. DATA FOR PRESSURE VS. VELOCITY

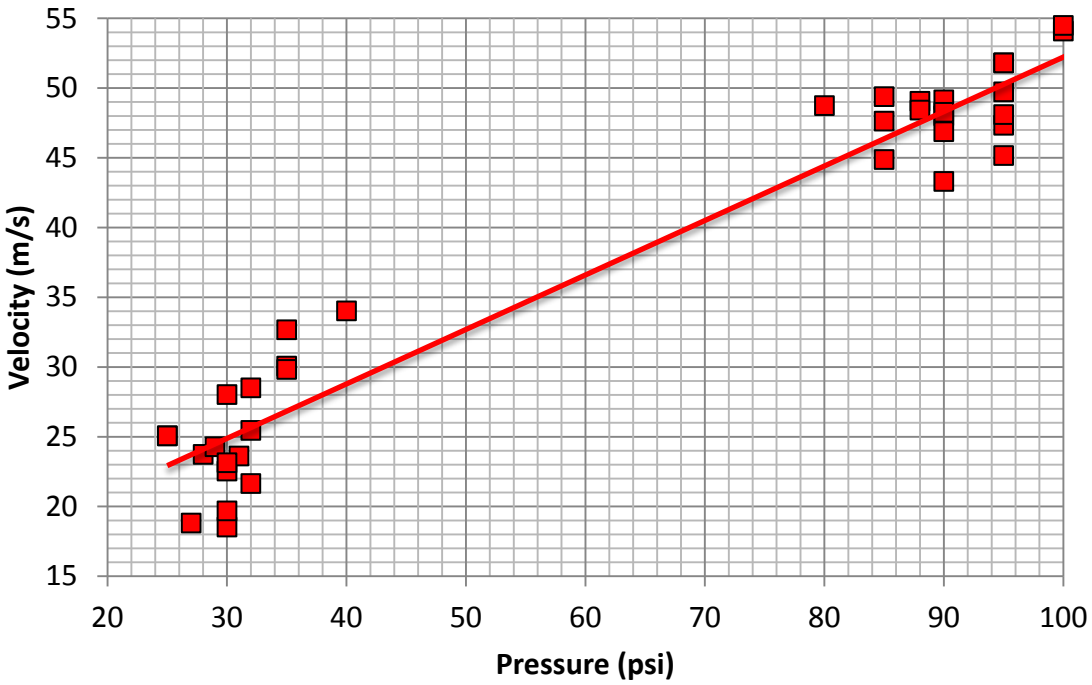

Low speed calibration data for 2.0 in. diameter SHI – average total projectile mass (sabot and SHI) 120.9 g, launched using nitrogen without burst membrane

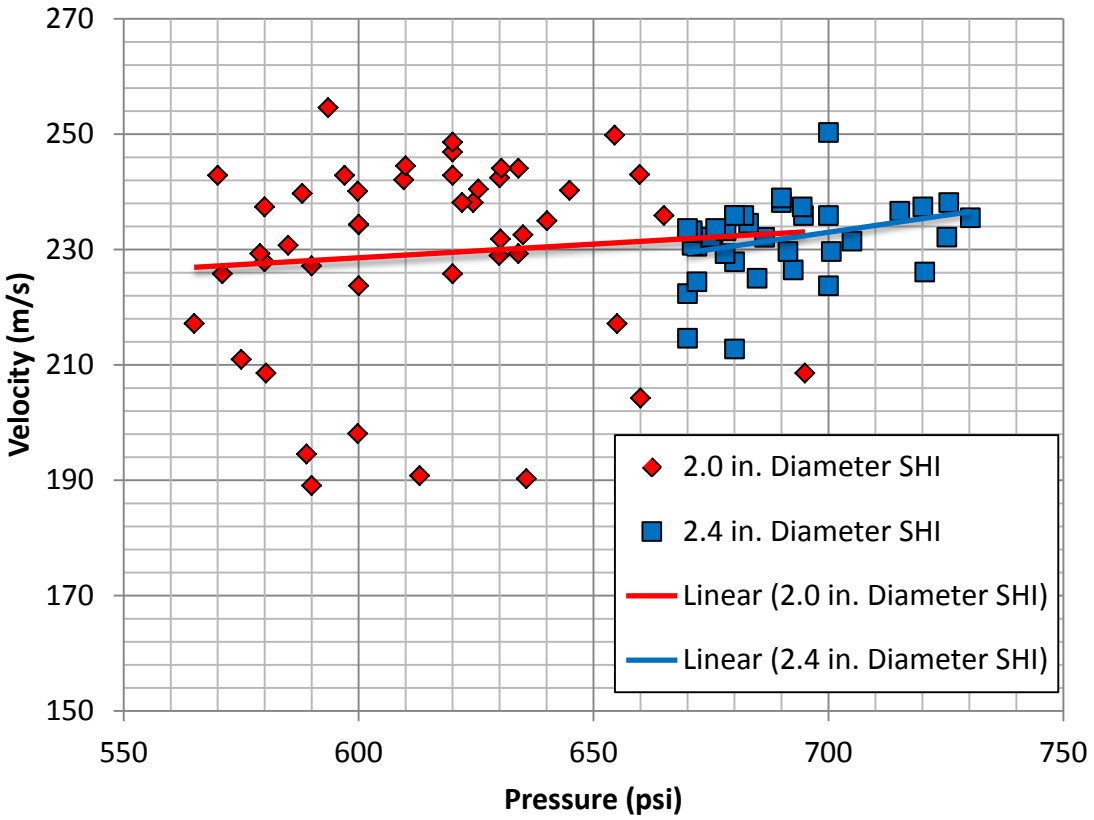

High speed calibration data for 2.0 and 2.4 in. SHI, both types were launched using helium gas with Mylar burst membranes – average total projectile mass (sabot and SHI): 124.7 g for 2.0 in. diameter, and 162.4 g for 2.4 in. diameter.